(2)

QUEST Technical Report No. 536

A PROFILING FIBER-OPTIC DIODE LASER DOPPLER VELOCIMETER FOR DEPLOYMENT IN COASTAL WATERS:

PROTOTYPE DEVELOPMENT

H.-T. Liu, P. D. Bondurant, W. T. Gustafson, M. H. Marvin,
R. A. Srnsky, C. R. Lentz, and R. F. Johnson

QUEST Integrated, Inc.
(formerly Flow Research, Inc.)
21414 - 68th Avenue South
Kent, Washington 98032

November 1991

Final Report

Prepared for

Office of Naval Research
Department of the Navy
800 North Quincy Street
Arlington, VA 22217-5000

Under Contract N00014-89-C-0308

SECURITY CLASSIFICATION OF THIS PAGE

REPORT DOCUMENTATION PAGE

Form Approved OMB No. 0704-0188

1a. REPORT SECURITY CLASSIFICATION Unclassified	1b. RESTRICTIVE MARKINGS
2a. SECURITY CLASSIFICATION AUTHORITY	3. DISTRIBUTION/AVAILABILITY OF REPORT Distribution unlimited; Approved for public release.
2b. DECLASSIFICATION/DOWNGRADING SCHEDULE	
4. PERFORMING ORGANIZATION REPORT NUMBER(S) QUEST Technical Report No. 536	5. MONITORING ORGANIZATION REPORT NUMBER(S)
6a. NAME OF PERFORMING ORGANIZATION QUEST Integrated, Inc. 6b. OFFICE SYMBOL (If applicable)	7a. NAME OF MONITORING ORGANIZATION DCMAO Seattle
6c. ADDRESS (City, State, and ZIP Code) 21414 - 68th Avenue South Kent, WA 98032	7b. ADDRESS (City, State, and ZIP Code) Bldg. 5D, NAVSTA Puget Sound Seattle, WA 98115-5010
8a. NAME OF FUNDING/SPONSORING ORGANIZATION Office of Naval Research 8b. OFFICE SYMBOL (If applicable) N00014	9. PROCUREMENT INSTRUMENT IDENTIFICATION NUMBER N00014-89-C-0308
8c. ADDRESS (City, State, and ZIP Code) 800 North Quincy Street Arlington, VA 22217-5000	10. SOURCE OF FUNDING NUMBERS PROGRAM ELEMENT NO. / PROJECT NO. / TASK NO. / WORK UNIT ACCESSION NO.

11. TITLE (Include Security Classification)
A Profiling Fiber-Optic Diode Laser Doppler Velocimeter for Deployment in Coastal Waters: Prototype Development (Unclassified)

12. PERSONAL AUTHOR(S) H.-T. Liu, P.D. Bondurant, W.T. Gustafson, M.H. Marvin, R.A. Srnsky, C.R. Lentz, and R.F. Johnson

13a. TYPE OF REPORT	13b. TIME COVERED	14. DATE OF REPORT (Year, Month, Day)	15. PAGE COUNT
Phase II Final Report	FROM 9/28/89 TO 9/30/91	November 1991	71

16. SUPPLEMENTARY NOTATION

17. COSATI CODES			18. SUBJECT TERMS (Continue on reverse if necessary and identify by block number)
FIELD	GROUP	SUB-GROUP	laser diodes, fiber optics, laser Doppler velocimeters, frequency shifting, backscatter, fast Fourier transform, FFT processor, Bragg cells

19. ABSTRACT (Continue on reverse if necessary and identify by block number)

A prototype profiling fiber-optic diode laser Doppler velocimeter (FODLDV) for flow measurement in coastal waters was developed, fabricated, and tested. The two-velocity-component FODLDV, a backscattered version of a field-proven diode laser Doppler velocimeter (DLDV), consists of a fiber-optic probe and link, an optronic module, a digital fast Fourier transform (FFT) based signal processor, and a data acquisition and control system (DACS). The fiber-optic probe and link are mounted on a traverse that facilitates velocity profiling up to a maximum range of 3 m.

(continued on reverse)

20. DISTRIBUTION/AVAILABILITY OF ABSTRACT	21. ABSTRACT SECURITY CLASSIFICATION
☒ UNCLASSIFIED/UNLIMITED ☐ SAME AS RPT. ☐ DTIC USERS	Unclassified
22a. NAME OF RESPONSIBLE INDIVIDUAL Alan Brandt	22b. TELEPHONE (Include Area Code) 202-696-4025 / 22c. OFFICE SYMBOL

19. Abstract (cont.)

The 1.6-cm diameter probe houses the collimating lenses attached to three single-mode polarizing preserving fibers, the focusing/receiving lenses, and a multimode fiber. The four 12-m-long optic fibers, protected in a water-tight armor cable, serve as the optical link between the probe and the optronic module; the single-mode fibers transmit the frequency-shifted laser beams to the probe, and the multimode fiber transmits the backscattered light back to the photodetector. The small-diameter FODLDV probe, with a total net laser power of 24 mW at 830 nm, allows the use of a short optical path of 8 cm without noticeable interference from the probe body. The components in the optronic module include the diode laser and controller, a three-way beam splitter, three Bragg cells and drivers, couplers for the optic fibers, and a photomultiplier tube (PMT) and driver. The signal processing system was designed utilizing a programmable digital signal processor (DSP) as the core computational unit. A 512-point FFT algorithm (8-bit frequency resolution) was developed and programmed into the DSP. The signal processor provides a burst digitization rate that can be varied from 1 MHz to 7.813 kHz in octave steps and has a continuously adjustable data rate from 10 to 200 Hz and variable demodulator frequencies (488 Hz steps) to accommodate asymmetric flows. To refine the validation process, three threshold levels of Doppler burst verification were adopted based on the signal and spectral amplitudes and on the signal-to-noise ratio (SNR) taken from the measured spectrum distribution. The processor is linked to the DACS, which consists of a miniature 80386-based PC, via a serial interface with a baud rate of up to 19200. Data are automatically recorded on the hard disk of the PC. Software packages were developed for both on-line monitoring and completely autonomous operation of the profiling FODLDV. The histogram and the 512-point spectrum distribution of the Doppler signal can be displayed on the screen in real-time and near-real-time paces, respectively. The above combination of medium laser power, a short optical path, and advanced signal processing is the key to operating the FODLDV in both clean and turbid waters. The traverse was designed for mounting the FODLDV on a stationary platform, operating in a move-stop-and-sampling mode. It may be modified to operate in a "yo-yoing" or "wave-following" mode. The controller of the traverse is also linked to the DACS via an RS-232 interface.

Command files allow all the operational parameters of the signal processor and the traverse to be modified on-the-fly. To operate the profiling FODLDV in an autonomous mode, a command file may be set up and executed to conduct an experimental sequence lasting for days, limited only by the capacity of the hard disk. A modified median filter (MMEDFILT) that incorporates an acceleration criterion was developed for effective removal of noise spikes inherent in laser Doppler velocimeter (LDV) signals. The implementation of the MMEDFILT has refined the application of laser anemometry by eliminating the "black art" approach to setting up the triggering threshold for signal validation. We have not only established a well-defined threshold for a given experimental condition but also lowered the threshold such that weak Doppler burst signals with a low SNR may be recovered and validated to boost the data rate.

The prototype was successfully tested in an oscillatory flow facility filled with tap water. A data rate of better than 90% has been achieved at a sampling rate of 200 Hz. The field deployment capability of the prototype has been successfully demonstrated.

TABLE OF CONTENTS

LIST OF FIGURES

ACKNOWLEDGMENTS

The authors wish to thank Dr. Y. C. Agrawal for furnishing useful suggestions throughout the Phase II investigation. Several of his suggestions have been incorporated into the design of the profiling FODLDV.

1. INTRODUCTION

To improve the development and maximize the utilization of naval weapons, it is necessary to understand the dynamic processes and the flow structures in the atmosphere, on the ocean surface, and in the ocean water body. Small-scale, high-frequency turbulence is one of the most important but least understood of these flow structures. Turbulence governs all the transport processes, in terms of mass, heat, and momentum, that play an important role in the ocean sciences, including physical oceanography, marine meteorology, coastal sciences, and air-sea interactions. A suitable field-worthy flow instrument with adequate frequency response and spatial resolution for field deployment in water and air is needed to obtain measurements of turbulent transport properties so that we can improve our understanding of these phenomena.

Laser Doppler velocimeters (LDVs) have been established as one of the most accurate and versatile instruments for nonintrusive velocity and turbulence measurements (Durst et al., 1976). LDVs are superior to many other velocity instruments with respect to wide dynamic range, fast dynamic response, high spatial resolution, linear calibration, stable or nondrifting characteristics, and applicability in air and water. In particular, LDVs are superior to conventional techniques for measuring multiple-phase flows as in the breaking wave zone where air bubbles are present (Liu and Lin, 1987). However, the applicability of LDVs in the field has been severely limited by their bulkiness and lack of portability.

These disadvantages have been overcome by the recent development at QUEST Integrated, Inc. (formerly Flow Research, Inc.), of a diode laser Doppler velocimeter (DLDV) for field deployment (Schedvin and Liu, 1984; Liu et al., 1985a, 1985b, 1989). In the compact DLDV, the bulky and power-hungry gas laser and peripherals of the conventional LDV are replaced by a miniature diode laser and optronic components. This development has revolutionized the application of the laboratory-proven laser velocimetry method to field conditions. The DLDV has been successfully field-tested in arctic waters under ice floes in two oceanographic expeditions (Liu et al., 1985a, 1989). Recently, a second-generation DLDV was developed in an attempt to remove the directional ambiguity of laser anemometry using a position-sensitive or lateral-effect (LE) photodiode (Liu, 1986; Liu and Bondurant, 1988) rather than Bragg cells, another step toward achieving portability of laser velocimetry for field deployment. In addition, simultaneous measurement of the speed, size, and concentration of sediment or airborne particles (Durst et al., 1976) may be achieved with laser anemometry.

The advantages of the DLVD as compared with the conventional LDV can be summarized as follows:

- Compactness and portability: All components of the DLDV are housed in two small water-tight modules, one transmitting and the other receiving (Liu et al., 1989). The entire volume of the DLDV is smaller than that of an equivalent 5-mW He-Ne laser alone. Further reduction in size may be achieved by incorporating integrated optronics (optics and electronics) in the design.

- Low electric power consumption: The laser diode is highly efficient and requires only low-voltage DC power. The DLDV may therefore be driven by batteries for an extended period of time, an attractive feature for field deployment (refer to Spectra Diode Labs [1988] manual).
- Long lifetime: The laser diode has an expected life of 50,000 hours. Replacement of the diode laser is a simple task. At present, the optical module of the diode laser (the laser diode, the collimator, and the beam shaper) is assembled as a unit or subsystem. This subsystem can be further miniaturized by using integrated optronics.
- Ruggedness for field deployment: The DLDV, which consists of all solid-state components, is much more rugged than its conventional counterpart, which uses a gas laser, and is better suited for deployment in hostile field conditions.

At present, continuous-wave (CW) index-guided laser diodes used in the DLDV have a maximum laser power of 30 to 100 mW at 780 to 830 nm (for those with single transverse and longitudinal modes). Such laser power is not adequate for measurements over a relatively long range (up to several meters), especially when operating in backscatter mode, which is necessary for optically scanning the focal volume to achieve the profiling function. Several options were considered in Phase I to determine the feasibility of configurations that could lead to the proposed development. (Refer to Liu [1989] for a more detailed description of the Phase I findings.) These options included:

1. Replacing the CW laser diode with a pulsed diode in order to take advantage of an increase of up to three orders of magnitude in the peak laser power.
2. Considering the development of a diode laser array velocimeter (DLAV).
3. Evaluating the use of a solid-state diode-pump YAG laser as the light source.

The Phase I investigation demonstrated that the first two options were not suitable for the proposed development due to inadequate coherent length of the pulsed laser diode and too few elements of the diode array. The third option had good potential to be used as the future laser source for field LDVs, provided high laser power in the hundreds of milliwatts is achieved. In particular, the visible YAG laser is preferable to the He-Ne or near-infrared lasers for oceanic measurements due to the significant reduction in the attenuation of visible light in seawater.

In addition to examining various laser light sources, we also assessed the optronic requirements during Phases I and II. It was determined that optically scanning an up-to-3-m range of a measuring volume (160-μm in diameter), formed by crossing at the waists of two 1.5-mm laser beams, placed extremely stringent demands on the precision and alignment of the optical components. Such demands may be difficult to meet even in the laboratory, let alone in hostile field conditions. For example, for measurements in an estuary, where the particulate concentration is high, multiple blockages of the laser light along the relatively long optical path (projection and collection) would be expected to significantly attenuate the already weak backscattered light to be sensed by the photodetector. Very high laser power would be required in such a case; otherwise, poor signal-to-noise ratio (SNR) would severely limit the scanning range of the LDV. However, scanning a high-power visible or near-infrared laser beam over

several meters would create a hazardous situation that would require special safety precautions. Technical and safety considerations thus dictate that maximum optical transmission be achieved by minimizing the optical path rather than maximizing laser power, particularly for applications in turbid water. This led to a decision to develop a profiling fiber-optic diode laser Doppler velocimeter (FODLDV) that employs a PC-controlled mechanical traverse with a range of up to 3 m to fulfill the profiling function.

In the last decade, fiber-optic laser Doppler velocimeters (FOLDVs) have been developed and made commercially available (by, for example, Dantec and TSI) for laboratory applications. These FOLDVs use either He-Ne or argon-ion lasers as the light source. The smallest fiber-optic head is approximately 1.5 cm in diameter with a focal distance of approximately 6 to 8 cm projected away from the focusing lens. A field FOLDV is, however, not commercially available. The first attempt to deploy a FOLDV (3.8-cm-diameter fiber-optic probe) in the field was made by Agrawal on the California Continental shelf in 1989; he upgraded a conventional autonomous field LDV (Agrawal, 1991) to a FOLDV using a 10-mW He-Ne laser as the light source. The FOLDV was later successfully deployed during the SUPERTANK experiments conducted in the wave tank at Oregon State University.

QUEST has developed a prototype of a profiling FODLDV for measuring spatial or temporal profiles of flows, turbulence, and current/wind shear in coastal waters. This development is a natural extension of the DLDV, requiring incorporation of a powerful diode laser and a profiling capability with the DLDV operating in a backscattered mode. The prototype FODLDV was extensively tested in the laboratory. In addition, the operation of the profiling FODLDV was successfully tested in the field.

In this report, the Phase II project is documented in full. First, the Phase II technical objectives are outlined in Section 2. Section 3 details the experimental methods and apparatus used in Phase II. Post-processing and analysis software developed for the FODLDV is described in Section 4, and the laboratory and field tests are documented in Section 5. Section 6 presents a summary of the Phase II research and development.

2. PHASE II TECHNICAL OBJECTIVES

The overall Phase II technical objective was to develop a prototype profiling FODLDV for the measurement of turbulence and currents in coastal and marine environments. A profiling range of up to 3 m was to be achieved using a PC-controlled traverse mounted on a stationary platform. The profiling FODLDV was to be tested and calibrated in the laboratory and deployed in the field.

Achieving this Phase II objective required that key subsystems of the profiling FODLDV be designed, fabricated, and integrated into a field deployable prototype system. Specifically, it was necessary to accomplish or establish the following:

- A DLDV with adequate optical power to operate in the backscatter mode and a photodetector optimized for detecting the weak backscattered light.
- A field deployable fiber-optic link: three single-mode polarization preserving fibers and one multimode fiber for transmitting the frequency-shifted laser light and collecting the backscattered light, respectively.
- An FFT based signal processor to measure and validate the Doppler frequency for two channels at a data rate of up to 200 Hz.
- A PC-controlled traverse with a profiling range of up to 3 m.
- A PC-based data acquisition and control system (DACS) with software for controlling the traverse, performing data acquisition in conjunction with the movement of the traverse, and recording the data on disks.
- Technical specifications of the profiling FODLDV to be determined through laboratory and field tests.

3. EXPERIMENTAL METHODS AND APPARATUS

During the Phase II research and development, our effort was to design, fabricate, and test a prototype field-worthy profiling FODLDV. A part of the groundwork for the proposed research and development had been established through the development of two generations of DLDVs (Schedvin and Liu, 1984; Liu et al., 1985b, 1989; Liu, 1986) and a field FOLDV (Agrawal, 1991) at QUEST. The experience gained in previous work was essential to the success of the present development, which was achieved by a combination of implementing innovative technologies, upgrading conventional optronics, and incorporating proven features of various versions of the above LDV systems.

3.1 PRINCIPLE OF LASER ANEMOMETRY

The operating principle of the LDV has long been well established (Durst et al., 1976). The proposed system adopts the dual-beam configuration by forming a sampling volume at the waists of the two focusing beams. Interference of the two highly coherent laser lights at the focal volume forms a set of dark and bright fringes whose pattern is parallel to the bisector and in the same plane as the two laser beams. Light scattered from small particles moving through the focal volume contains the Doppler frequency information; this a measure of the fluid velocity component in the direction perpendicular to the fringe pattern. The relation between the Doppler frequency and the velocity vector of the particles is

$$f_D = \mathbf{u} \cdot (\mathbf{k} - \mathbf{l}) / \lambda \tag{1}$$

where f_D is the Doppler frequency, $\mathbf{u}$ is velocity vector, $\mathbf{k}$ and $\mathbf{l}$ are the unit vectors of the two incident beams, and λ is their wavelength. Then, since $|\mathbf{k} - \mathbf{l}| = 2 \sin \phi$

$$f_D = 2 u_x \sin \phi / \lambda \tag{2}$$

where ϕ is the half angle between the two beams and u_x is the velocity component perpendicular to the bisector of the two beams. The fringe model is developed based on the observed fringe pattern. From the geometry of the laser beams, the fringe spacing, d_f, is given by

$$d_f = \lambda / (2 \sin \phi) \tag{3}$$

Therefore, Eq. (2) may be given in an alternate form relating the fringe spacing to the particle velocity component:

$$u_x = d_f f_D \tag{4}$$

From Eq. (4), the inverse of the fringe spacing corresponds to the calibration of the LDV in kHz/(cm/s) or MHz/(m/s) depending on the dimensions chosen.

To remove the 180° directional ambiguity inherent in laser anemometry, dual Bragg cells were used to achieve a net Doppler frequency shift, creating a "running" fringe pattern at the focal volume. This enables us to measure the negative velocity component corresponding to a Doppler frequency up to

the net frequency shift. With the use of the Bragg cells we can also use a three-beam configuration forming two perpendicular focal volumes to measure two velocity components. The net frequency shifts of the three beams must have large separation so that they may be isolated (the two perpendicular pairs) or discarded (the third pair) effectively via band-pass and low-pass electronic filtering.

3.2 PROFILING FODLDV COMPONENTS AND APPARATUS

In essence, the profiling FODLDV consists of five key subsystems--namely, a fiber-optic probe and link, an optronic module, a digital signal processor (DSP) based FFT processor, a PC-based DACS, and a PC-controlled traverse (Figure 1). The optronic hardware is housed in an instrument cabinet on casters with a total of three decks--two 19-in. (48-cm) rack-mount drawers and a bottom deck. The FFT processor/DACS and the optronic module occupy the two drawers. Several power supplies and controllers are mounted on the bottom deck. In this section, we describe in detail these subsystems and their integration. Other experimental methods and apparatus used in Phase II are also documented.

3.2.1 Fiber-Optic Probe and Link

The fiber-optic probe and link consist of optical components that transmit and project the laser beams to form the focal volumes in the fluid and collect and deliver the backscattered light back to the photodetector. The components of the probe are housed in a water-tight aluminum cylinder with an outside diameter of 1.6 cm. Figure 2 is an engineering drawing of the probe, which is attached to one end of the fiber-optic link. The fiber-optic link consists of four fibers, three single-mode and one multimode, which are housed in a water-tight armor cable with an outside diameter of 1.6 cm.

Each of the three frequency-shifted laser beams exiting the Bragg cells is coupled to one of the three 12-m long, low-loss, single-mode polarization preserving optic fibers (Fujikura). At the probe end, collimators are attached to the fibers emitting laser beams with diameter $D_{e^{-2}} = 0.4$ mm. The collimators are carefully aligned and supported in the probe housing to form three parallel beams that are focused via a coated achromatic lens (focal length $f = 60$ mm in air). In water, the three beams form a common focal volume at 75.6 cm from the front surface of the achromat. Beams 1 (Bragg-shifted 80 MHz) and 2 (81 MHz) and Beams 2 and 3 (85 MHz), with respective net shifts of 1 and 4 MHz, form the two focal volumes and facilitate the measurement of the two mutually perpendicular velocity components. The separation d between Beams 1 and 2 and Beams 2 and 3 is 5.66 mm. The half angle between each of the two beams is 2.70 degrees. For the FODLDV equipped with a 830-nm laser diode and with laser beam diameters of 0.4 mm, the diameter of the focal volume $d_{e^{-2}} = 4 \lambda f / \pi D_{e^{-2}}$ μm. The corresponding length of the focal volume $l_m = d_{e^{-2}} / \sin \phi = 3.4$ mm. From Eq. (3) the fringe spacing is calculated to be 8.8 μm and the conversion factor is 1.135 kHz/(cm/s). Assuming Gaussian laser beams, the number of fringes is estimated to be NFR = $1.27d / D_{e^{-2}} \simeq 18$. Refer to Durst et al. (1976) for detailed derivations of the geometry of laser anemometry.

To collect the backscattered light from particles moving through the focal volume, the same focusing lens serves as one of the two collecting lenses. A second lens identical to the first lens but with

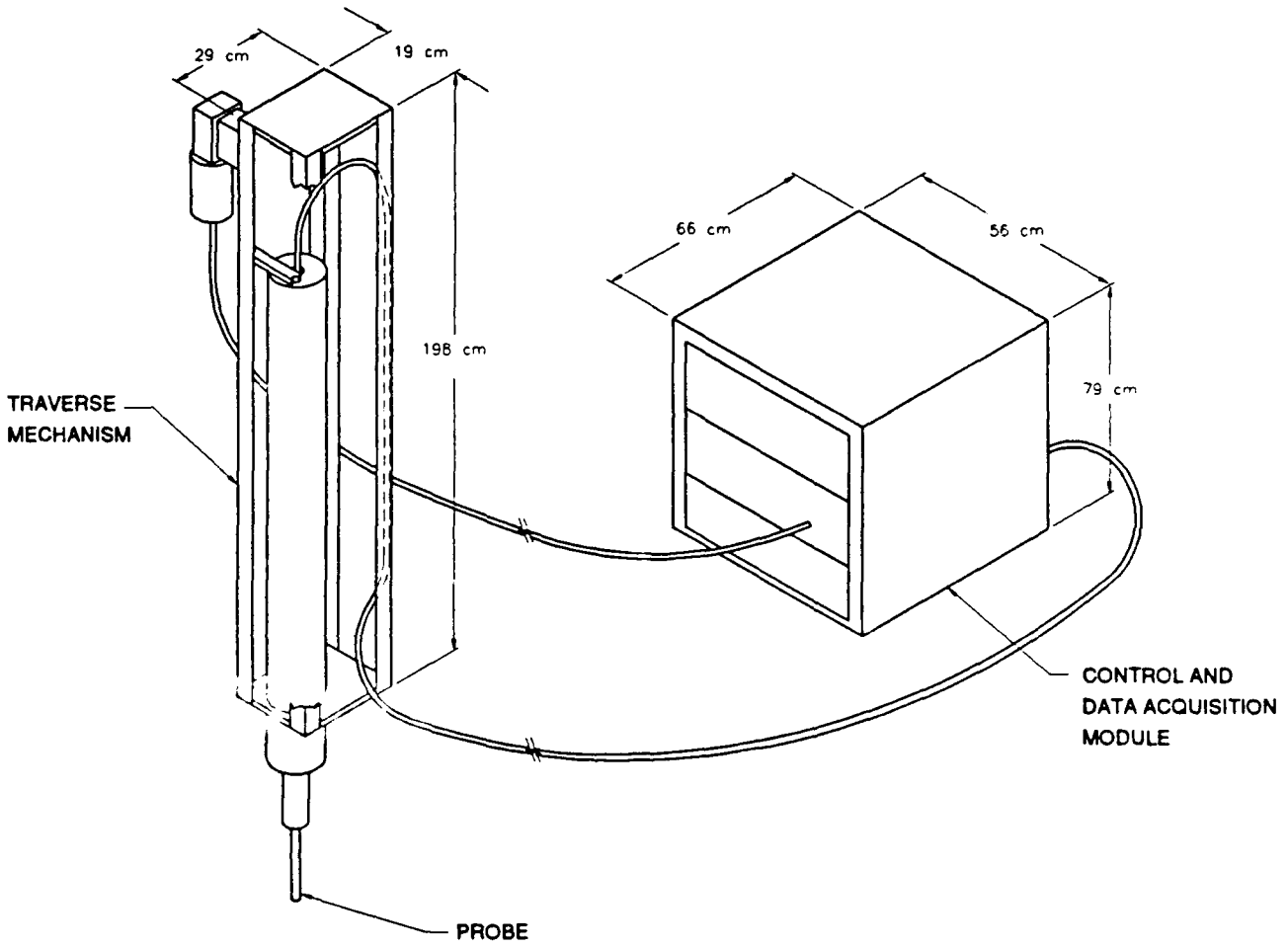

Figure 1. Overall Assembly of the Profiling FODLDV

a smaller diameter focuses the backscattered light from particles passing through the focal volume onto the tip of a 12-m-long multimode fiber through which the light is transmitted to a photodetector in the optical module. The second lens was notched at three locations (Figure 2) to allow unobstructed passage of the outgoing laser beams to be focused by the first lens.

3.2.2 Optronic Module

The optronic module includes the diode laser, the beam splitter, the Bragg cells, the photodetector, the fiber-optic couplers, and their controllers or drivers. Figure 3 illustrates the layout of key elements of the module in a 19-in (48-cm) rack-mount drawer. The diode laser, the three-way beam splitter, the Bragg cells, and the fiber-optic couplers are mounted on a single 1.27-cm-thick aluminum back plate to maintain the optical alignment once optimized.

Diode Laser

The diode laser consists of a 100-mW index-guided laser diode (Spectral Diode Labs, Inc., Type 5412-H1) mounted on a heat sink and a set of beam shaping and collimating optics (Liu and Bondurant, 1988). When the diode is operating at 25°C, the wavelength of the emitted laser light is 830 nm, according to the manufacturer's specifications. There is a power loss of approximately 15% through the optical elements, resulting in a laser power of about 85 mW. The output laser beam is approximately circular with a diameter of 1 to 1.5 mm. The maximum beam divergent angle is less than 1.3 mrad.

The laser diode is driven by a laser-diode controller (ILX Lightwave, LDC-3722) offering both fine control of low noise and highly stable current output (±2 mA accuracy) and temperature (±0.2°C accuracy). Such fine control is essential for stabilizing the wavelength and for prolonging operating life up to its full potential (50,000 hours). The controller is mounted on the bottom deck of the instrument cabinet.

Beam Splitter

The three-way beam splitter is composed of two prisms and a 30/60 and a 50/50 1.0-cm cube beam splitter (Melles Griot) to achieve a 33% splitting of the incoming laser beam (see Figure 3). The prisms and beam splitter cubes are sandwiched between two aluminum plates equipped with pin locators to maintain their relative positions. The surfaces of the optical elements are coated with anti-reflection layers optimized for 830 nm light.

Bragg Cells and Drivers

Three Bragg cells or acoustic-optic modulators (Newport EOS N23080-3) driven by individual controllers (N21080-6AMXTAL) with crystals operating at 80, 81, and 85 MHz are bolted on aluminum angles which are pin-mounted on the back plate. A set screw between the angle and the plate facilitates a fine rocking adjustment of the cell for aligning the aperture with the incoming laser beam. An opposing

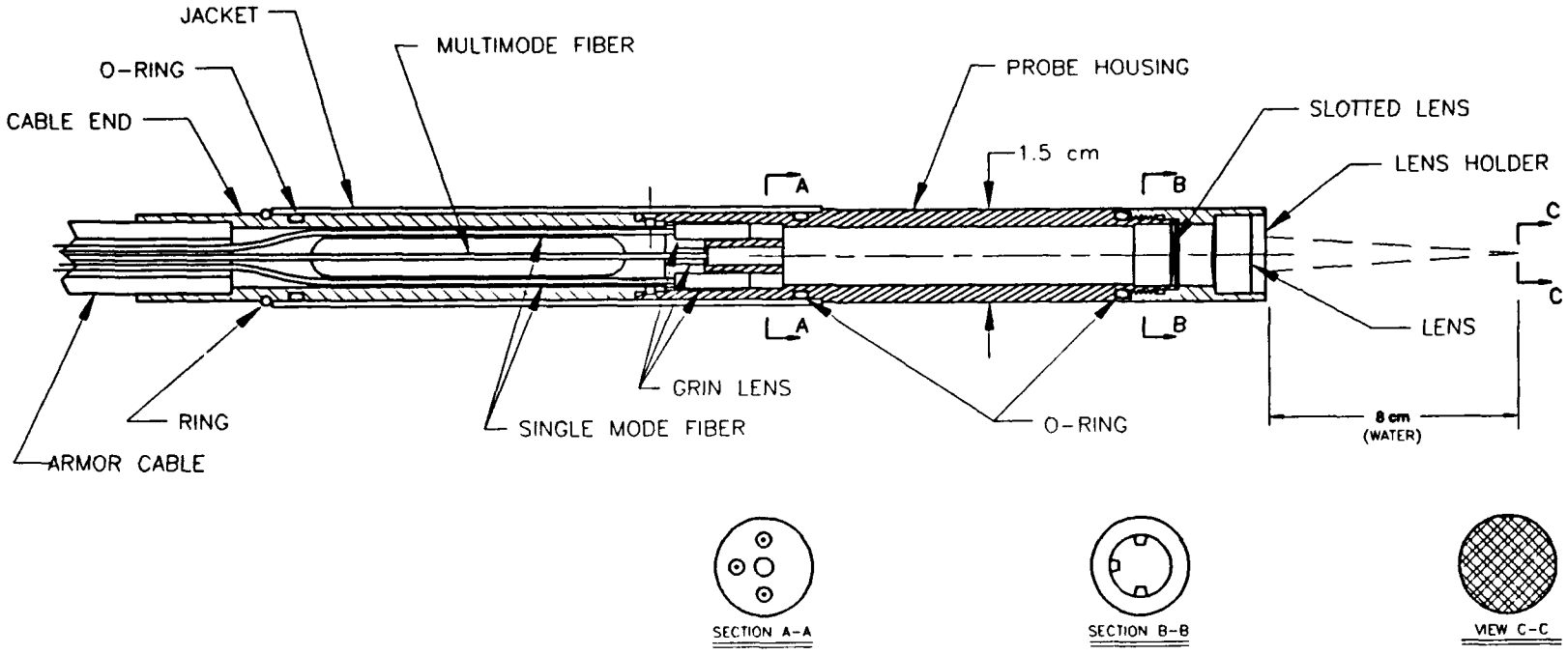

Figure 2. Fiber Optic Probe and Link

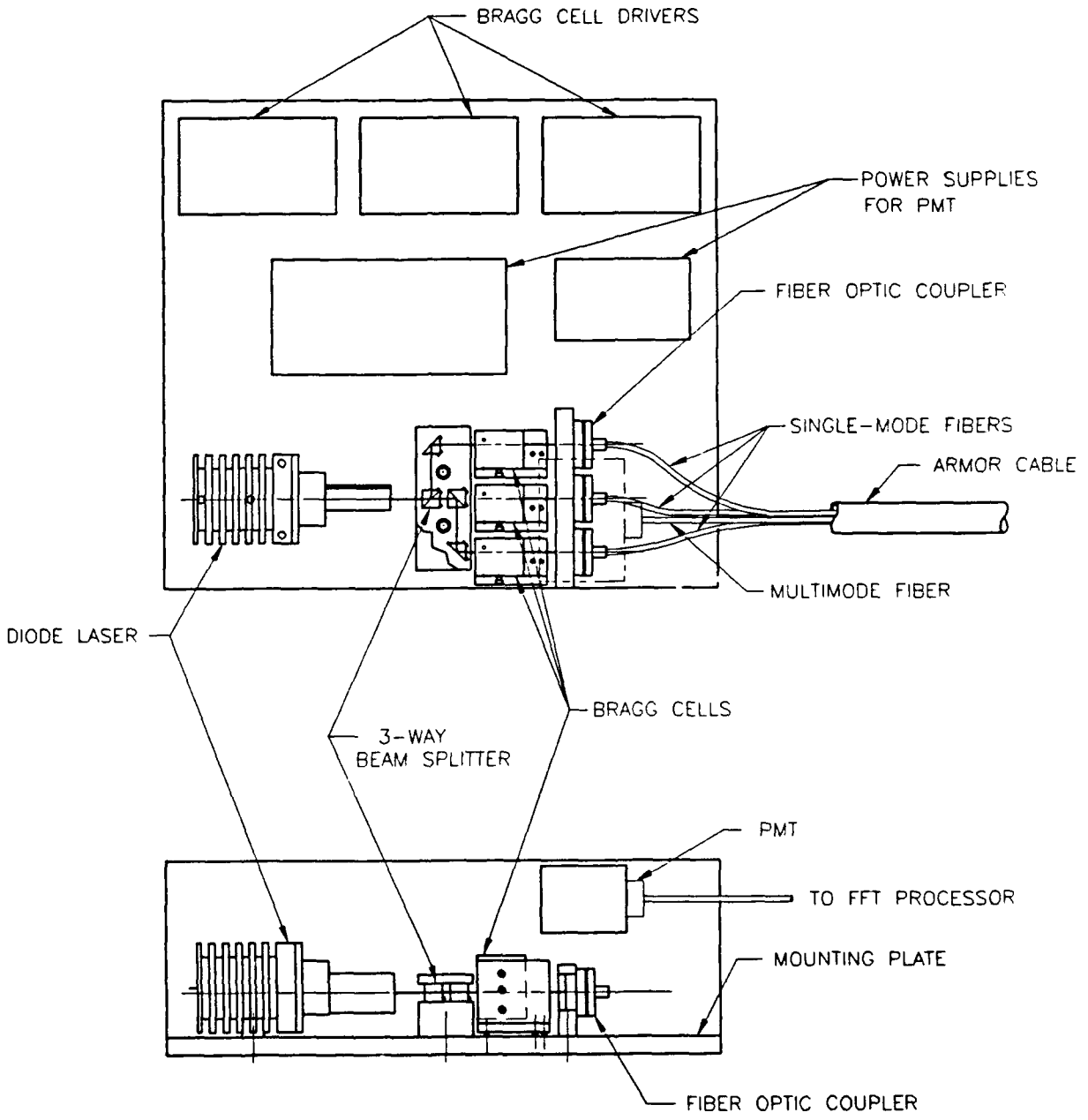

Figure 3. Optronic Module

set screw locks the Bragg cell into position once its orientation is optimized. The optical efficiency of the Bragg cells is about 75%. The output first-order beams with respective frequency shifts of 80, 81, and 85 MHz have a total power of about 64 mW.

Fiber-Optic Couplers

Three fiber-optic couplers (OZ Optics) for the single-mode fibers are mounted downstream of the Bragg cells. Displacement and tilt adjustment via a combination of an O-ring and three set screws on the couplers is provided to maximize the coupling of the first-order shifted beams to the fibers. The coupler may then be locked into position via another three set screws. The efficiency of the coupler is better than 35%. After laser light passes through the 12-m fibers and the grin lens with a very small amount of loss, the total net laser power of the collimated beams is 24 mW. This results in an overall optical efficiency of 24% for all the optronic media for shaping, transmitting, and processing the laser light emitted from the 100-mW laser diode.

Photodetectors

Several photodetectors were tested to detect the backscattered light from particles passing through the focal volume of the prototype FODLDV; the one with the optimum performance was selected for the prototype. The first one tested was an Avalanche photodiode (APD) by Hamamatsu (NDL1102). The APD has an active area with a diameter of 250 μm, which requires precision alignment of the fiber and the active area for maximizing light detection. The small area is necessary to minimize the shot noise. The APD has a quantum efficiency of better than 75% at 830 nm. A complete detector system including the APD, the driver circuitry, the power supply, and the housing is available from TSI (Model 9150A). The system has a bandwidth from DC to 9 MHz at -3 db.

The second and third detectors tested were Hamamatsu R928 and R636 photomultiplier tubes (PMTs). The R928 and P636 have a quantum efficiency of approximately 1% and 8%, respectively, at 830 nm. The PMT generally has a large active area such that precision alignment is not necessary. Both require a high voltage supply up to 1250 V. A potentiometer is provided for adjustment of the voltage supplied to the PMT.

Extensive tests of the photodetectors have demonstrated that the PMT is superior to the APD in that the shot noise of the latter is significantly higher while the gain is lower than that of the former. Among the two PMTs, the R636, with relatively high quantum efficiency, performed even better than the R928. The high shot noise in the form of very sharp, large-amplitude voltage spikes present in the APD signals constantly triggers the FFT processor and results in a significant reduction in the data rate (see Section 4). In addition, the significantly higher gain of the PMT compared to the APD enhances the performance of the FODLDV for measurements in water bodies with very low particle concentrations--e.g., in tap water or arctic waters (Liu et al., 1985).

3.2.3 Signal Processor

The signal processor developed under this contract was based on the work done originally by Agrawal and Belting (1988) using the chirp-Z method of calculating the Fourier transform (Agrawal, 1984) of the Doppler burst. The modified chirp-Z based processor continuously sweeps across the spectrum of the incoming signal and, using analog electronics, determines the location of the spectral peak. The location of the spectral peak relative to the entire sweep is saved and presented as the velocity data. This approach has the twin advantages of being completely insensitive to signal drop-out (as opposed to phase-locked-loop trackers) and being ideal for low SNR applications (unlike the counter processor, which is suitable for intermittent signals but requires high signal quality). The processor has been used in the deep sea (Agrawal and Belting, 1988) and in shallow water (Agrawal et al., 1988). The former application exemplified a low-data-rate situation; the latter, a continuous-signal situation. The same principle has been applied in more recent commercial LDV processors, but they are an order magnitude more expensive.

The signal processor developed under this contract provides a higher level of functionality and much greater versatility than the original Fourier transform processor described above. The disadvantages of the chirp-Z Fourier transform circuitry are primarily power consumption and size. Each chirp-Z transform card requires 10 to 12 W of power and consists of one 11.5-in. x 5-in. circuit card and two smaller piggy-back circuit cards. As originally designed by the manufacturer, the full-scale frequency range of the chirp-Z card is $\pm$31.25 kHz with a clock speed of 2 MHz. To accommodate higher velocity flows, the clock speed has been increased to 12 MHz, providing a full scale frequency range of $\pm$187.5 kHz at the expense of increased noise and lower input signal dynamic range. There is also an extensive adjustment procedure that should be performed each time the clock frequency is changed. The chirp-Z card thus does not lend itself to being incorporated into a frequency-agile system where the system sample rate can be modified to maximize resolution in a given flow field.

Figure 4 illustrates the primary components of the FODLDV signal processor and how they are tied together. The output of the PMT (or APD) is first processed by the demodulator card, where it is broken into two signals, one for each measurement axis. The two output signals are then converted to the frequency domain by two identical FFT processors that operate in parallel. The burst data from each axis are validated independently in each FFT processor. The FFT interface card provides data buffering and a high-level command interface to the demodulator card and the two FFT processors. The physical interface to the signal processing package is via a selectable-baud-rate RS-232 serial interface. All high-level commands and burst data are transferred via this interface. All four cards are plugged into an industry-standard G-96 bus, and it is through this bus that the FFT interface card communicates with the other three cards. Each circuit card is 4 in. wide by 6.5 in. long and less than 0.75 in. thick. The total power consumption of the four cards is less than 10 W. A more detailed discussion of each circuit board is provided in the following paragraphs.

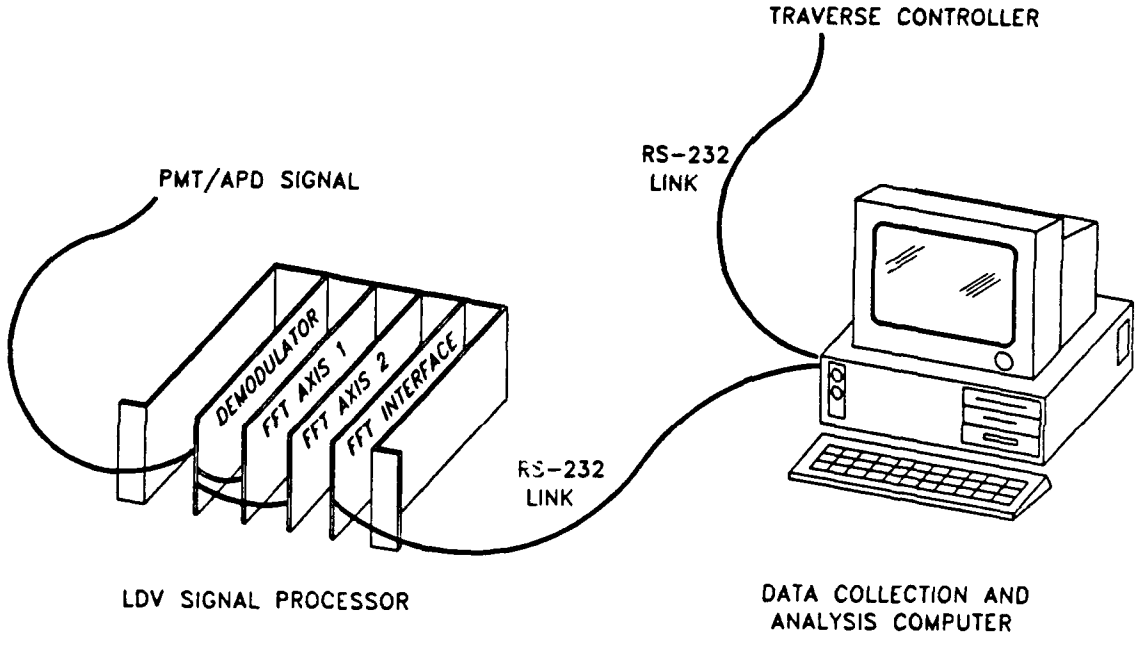

Figure 4. FODLDV Signal Processor

Demodulator Card

The block diagram for the demodulator card is shown in Figure 5. The signal from the detector is the sum of two signals, one from each measurement axis, separated in the frequency domain. The frequency separation is a function of the differences between the Bragg cell drive frequencies, which, for this system, are nominally 1 and 4 MHz. The detector signal is split and band-pass filtered (BPF) to separate the signal into the 1 and 4 MHz components. The band-pass filters are centered on 1 and 4 MHz with a bandwidth of 500 kHz. This is compatible with the maximum sample rate used by the FFT processors and allows the Doppler frequency to vary a maximum of ±250 kHz about the zero particle velocity frequency. After band-pass filtering each signal is mixed with the output from a programmable oscillator. This shifts the frequency of the Doppler signal to within the frequency measurement range of the FFT processors. The programmable oscillators are variable from 0 Hz to 32 MHz in 488 Hz steps. This allows placement of the zero particle velocity anywhere within the measurement range of the FFT processor to optimize the frequency resolution for asymmetric flows. Once the frequency of the two channels has been shifted, each is routed through a low-pass filter to prevent aliasing before the signal is digitized on the FFT processor card. The filter is programmable to provide optimal filtering for the various digitization rates on the FFT processor. The programmable oscillator and filter frequencies are controlled via the G-96 data bus connection on the circuit card and are accessible by the FFT interface card across the bus. To achieve the small size of the demodulator card, a four-layer printed circuit card was designed with the ground and power planes as the center traces. Surface-mount components were used where possible to shrink the board size further.

FFT Processor Card

The block diagram of the FFT processor card is shown in Figure 6. When the amplitude of the Doppler burst from the demodulator card exceeds a preset programmable threshold, the analog-to-digital (A/D) converter converts 512 data points and stores them in a first-in-first-out (FIFO) data buffer. The digitization rate is selectable from 7.8125 kHz to 1000 kHz in octave steps to allow a wide variety flow variations and resolutions. The burst data are stored in the buffer until the TMS320C25 DSP is interrupted by the FFT interface card (via the G-96 bus) and instructed to calculate the spectrum. This interrupt is done periodically and sets the basic data rate of the system. It can be adjusted to any value between 10 Hz and 200 Hz. After each interrupt, the DSP quickly moves the burst data from the FIFO into data memory and re-enables the trigger circuitry to capture the next burst. The DSP then normalizes the data and calculates the spectrum. The burst is validated using two different criteria: the peak of the power spectra must exceed a preset threshold, and the ratio of the spectral peak to the average spectral level must exceed a preset threshold level. Both criteria must be met for the burst to be considered good. In addition to calculating the burst frequency, the FFT processor also calculates the time between the last interrupt from the FFT interface card and the time of the burst. This allows the occurrence time of each burst in the data record to be determined during post-processing. This information can be used to provide a less noisy estimate of the wave spectra.

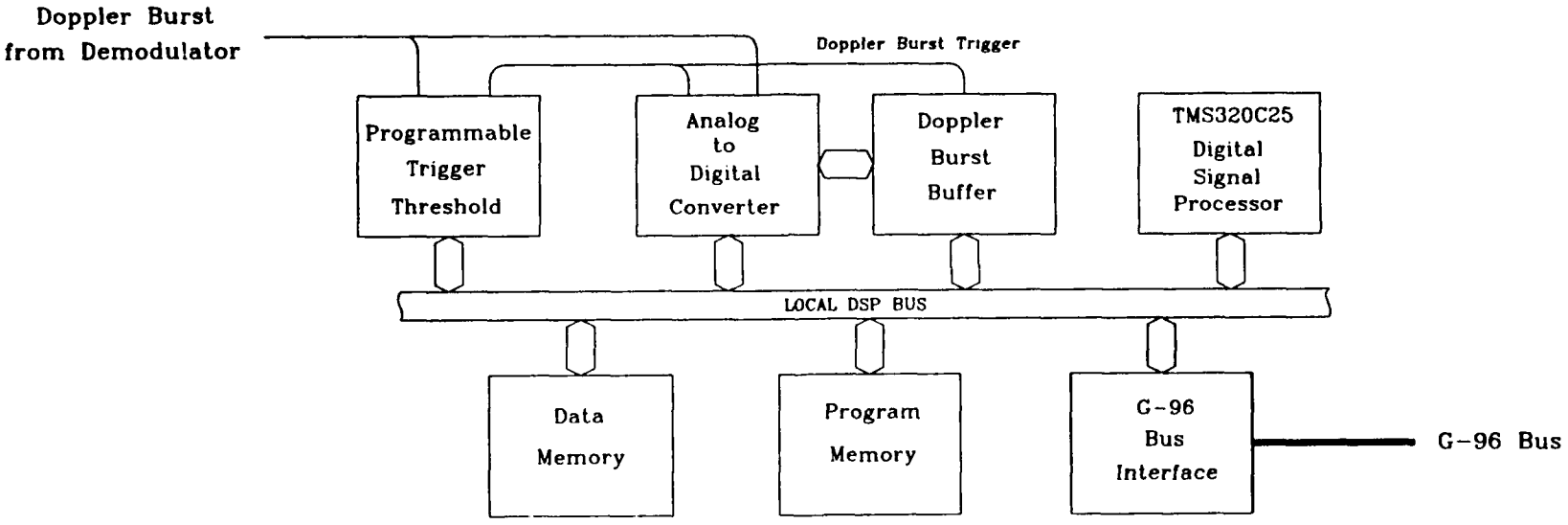

Figure 5. FFT Processor Card Block Diagram

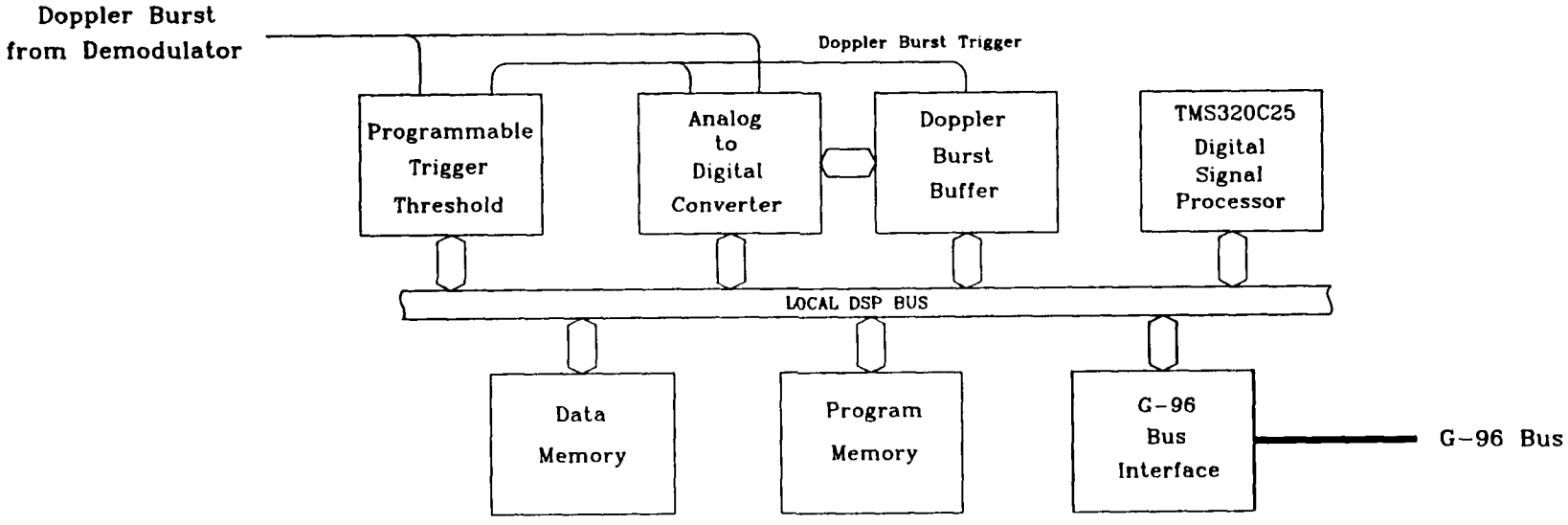

Figure 5. FFT Processor Card Block Diagram

The software for the FFT processor card is written in assembly language and is broken into four different modules with approximately 2100 lines of source code. The psdldv.asm module is the main control routine that handles the communications with the FFT interface card, initializes and performs diagnostics, and is the control loop for processing the Doppler bursts. A summary of the commands used between the FFT processor card and the FFT interface card is provided at the end of Appendix A. The init-fft.asm and c2cx0256.asm modules are the initialization and core processing routines to implement a 256-point complex-in/complex-out, radix-2 decimation-in-time FFT routine. The tonxform.asm module is based on a method described in Brigham (1974) to post-process the output from a 256-point complex transform to generate a 512-point FFT (8 bits of frequency resolution). This process requires that the odd input data samples be used as the real component of the complex input to the 256-point FFT and the even input data samples be used as the imaginary components.

Diagnostics are embedded in both the hardware and software of the FFT processor. Each time the power is applied to the system, an extensive set of diagnostics is performed and the results are presented to the FFT interface card. This includes memory testing, timer/counter testing, processor functionality, and calculation of the spectrum of a test signal. A simple test signal is automatically switched to the input of the FFT processor during diagnostics to simulate a Doppler burst. The FFT processor calculates the spectrum of this test signal just as if it were a normal burst. This also tests the burst trigger circuitry, A/D converter, and FIFO. All of the diagnostics described above are performed simultaneously on both FFT processors right after power is applied to the system.

FFT Interface Card

This card is a commercially available Gespac model MPL-4079 68HC000-based microprocessor card with the following features:

- Two RS-232 serial ports
- Two 16-bit timers and 20 TTL I/O lines
- Four-channel, 8-bit A/D converter
- Battery-backed, 256K CMOS random-access memory (RAM)
- Battery-backed real-time clock/calendar
- Low power consumption, 50 mA and +5 V only operation
- G-96 bus interface

The serial port allows transfer of data and commands between the signal processor and the DACS. The data transfer rate is selectable among 1200 baud, 9600 baud, and 19.2 Kbaud. The commands that are sent via this cable to the FFT interface card are two-character ASCII commands typically followed by numeric arguments. A complete list of commands is provided in Appendix A. The timer on this card is used to generate the periodic interrupt discussed in the FFT processor section of this document. In the current configuration of the system the 20 TTL I/O lines, battery-backed clock, and A/D converter are not used. They could be used to collect auxiliary inputs such as status bits and output from pressure sensors, anemometers, etc. in situations where the DACS is not provided or not needed with the system. If the

256K, battery-backed RAM is not sufficient for local data storage, additional memory can be added via the G-96 bus. The FFT interface card plugs into the G-96 bus where commands and data are sent to the two FFT processors and the demodulator card. These can be commands originating from the RS-232 serial port or internal diagnostic commands such as those used during power-up.

The software to control this board is written in C using the 2500AD cross-compiler and consists of approximately 3400 lines of source code across five modules. The primary function of the software is to provide a high-level interface to the signal processor in the form of simple two-character commands. In addition it provides data buffering and storage in the case where the data cannot be off-loaded from the signal processor as fast as the data are generated by the FFT processors. Additional memory can be added if necessary to increase the buffer area.

3.2.4 Data Acquisition and Control System

The data acquisition and control system is an IBM PC-compatible AMPRO Little Board 386 computer. It is configured with 1 Mbyte of memory, a 104-Mbyte hard disk, a 3.5-in. floppy drive, two serial ports, one printer port, and a video graphics array (VGA) display card. The computer is very compact and is the size of a standard half-height floppy disk drive and as such fits in the same 19-in. rack as the signal processor and the GALIL motion controller. The computer interfaces with the rest of the system via the two serial ports. One serial port is used to send commands and receive data from the signal processor, the other is used to interact with the GALIL motion controller that drives the traverse mechanism. The operator interfaces with the computer via a standard VGA monitor and PC keyboard, both of which can be removed when the system is configured with command files for autonomous operation.

The primary functions of the DACS are:

- To coordinate and synchronize the actions of the signal processor and traverse mechanism for data collection and storage.
- To provide methods for displaying data in real time to aid in configuring the system for experiments.

The system is designed to allow both manual and autonomous operation. Appendix A provides a complete description of the commands used to control the signal processor, and Appendix B summarizes the commands that are used to control the traverse mechanism. The letter "G" must be added as a prefix to the two-letter commands listed in Appendix B; the "G" instructs the DACS software to route the command to the GALIL traverse controller instead of to the signal processor. To simplify manual operation as well as facilitate autonomous operation, command files are provided to automate command sequences. Each command file is prefaced with a time-and-date stamp that tells the computer when to execute the command file using the clock/calendar built into the DACS as the time reference. Any command that can be manually executed from the keyboard can be placed in the command file, including both traverse commands and signal processor commands. Command files can also be used to automatically set a particular combination of parameters. This reduces the tedium of remembering a

particular threshold value or a particular combination of parameters. For the field experiments performed during this contract, command files were used to automate the collection of velocity profiles. At the beginning of each command file, the threshold and validation levels for each FFT processor were set as were the traverse control parameters such as velocity and acceleration. Once the system is initialized, collect-data commands are alternated with traverse-move instructions. The velocity data from each traverse depth is automatically stored to the hard disk after each data collection and between traverse moves. If needed, the burst trigger thresholds (ST command), burst validation thresholds (SL & SV commands), and data rates can be optimized for each velocity measurement depth.

The DACS computer also provides a method for displaying data in real time and near-real time. This is used primarily for setting the burst trigger and validation thresholds and for making quick assessments of the performance of the system. The spectral display plots in near-real time the spectrum of the most recent burst from the selected measurement axis. The vertical axis units are the same as those used to set the spectral-level validation threshold (SL command). The spectrum display also calculates and displays the ratio of the current spectral peak to the average spectral noise level and is used to help set the signal-to-noise validation threshold (SV command).

The second display is a real-time histogram of the velocity data currently being collected. Those data samples that meet both the spectral-level validation threshold (SL) and the signal-to-noise threshold (SL) are plotted in blue; those samples which do not meet the validation criteria are plotted in red. At the end of the data collection process, the red data points are removed from the graph data set and the graph is scaled and re-graphed.

3.2.5 Mechanical Traverse

The traverse (as illustrated in Figure 7) was designed to be handled comfortably by two persons (it is 2 m tall unfolded and weighs 52 kg). The maximum traversing distance is 3 m. At present, the traverse is designed to operate in the move-stop-and-sample mode. In other words, data are in the form of time series taken at fixed distances below the mean ocean surface for a period of time (say, 2 min). The traverse may be modified to operate in the "wave following" or "yo-yoing" mode.

The traverse consists of two telescoping tubes supported by a frame made of aluminum angles. All components of the mechanism are made of corrosion-resistant materials--namely, aluminum, stainless steel, or plastic. The telescoping action serves two functions: compactness and stiffness. When in the retracted position, the traverse is only 2 m tall, yet it will traverse 3 m. The inner tube is 60 mm in diameter and is supported by ball bearing guide wheels at the bottom end of the outer tube. The outer tube is 115 mm in diameter and is supported by ball bearing guide wheels at the bottom end of the aluminum angle frame. The outer tube is driven by a dual-cable chain system on a single drive shaft. The cable chains are situated in a protected area of the aluminum angle frame to prevent damage from foreign objects. The drive shaft is coupled to an electric motor through a 50/1 worm gear reducer. The

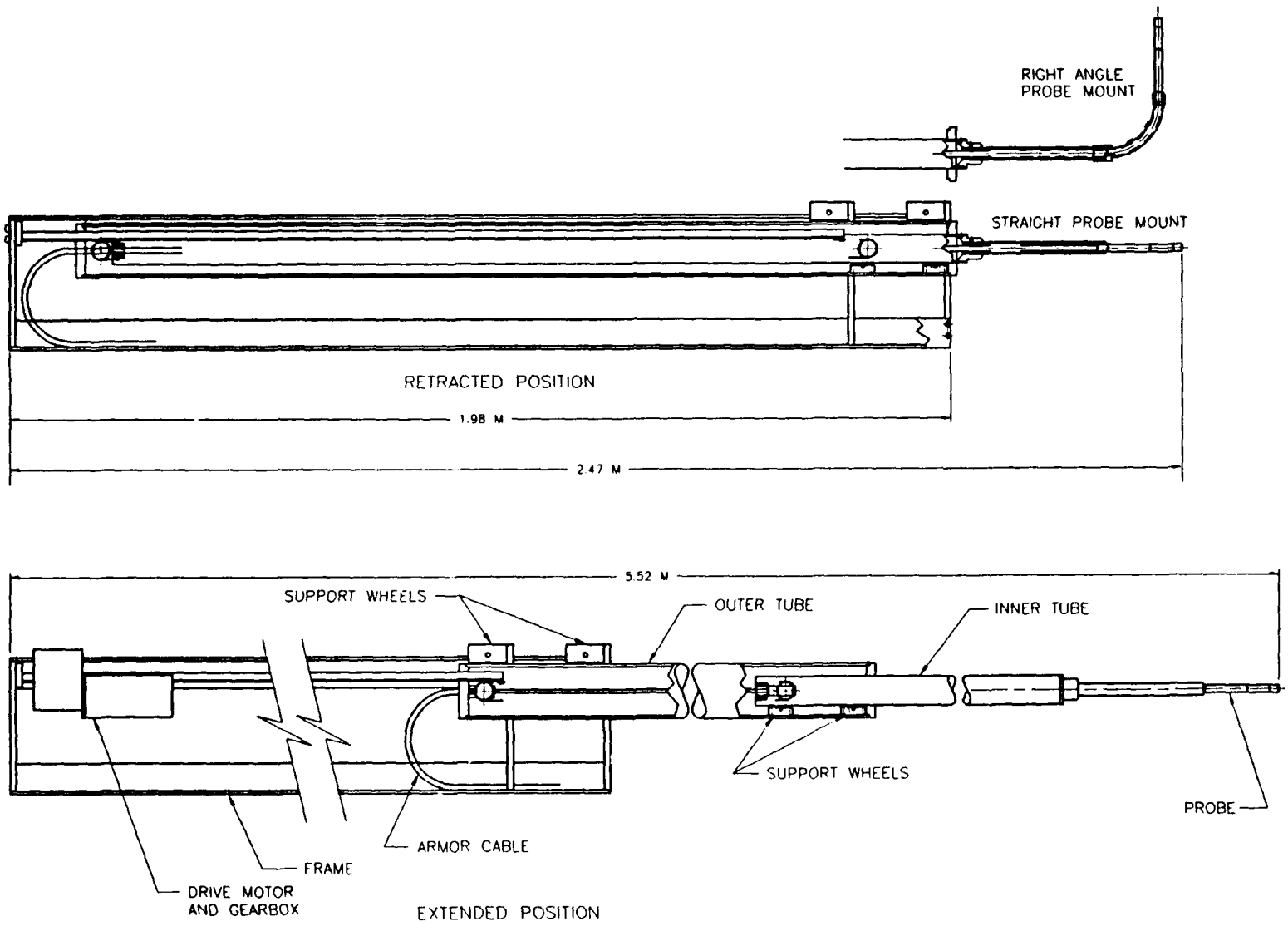

Figure 7. Details of the Mechanical Traverse

motor and gearbox are sealed to prevent water intrusion. The inner tube is driven by a motion-doubling system such that it moves twice as fast as the outer tube. The fiber-optic probe and link and armor cable are removable from the traverse assembly for shipping. The probe may be mounted with its axis parallel or perpendicular to the traverse axis depending on the velocity components to be measured. All electrical wiring and components are in sealed enclosures and conduits in order to provide protection from water.

The traverse is equipped with a DMC-400 DC motor controller manufactured by GALIL Motion Control, Inc. The feedback comes from an incremental encoder; no additional velocity feedback is required. The DMC-400 controls the motor position. A set of instructions, consisting of two-letter commands sometimes followed by a number, facilitates the programmable control capability. The motion commands are along trapezoidal velocity profiles where the acceleration and the slew rates are programmable. A number of the commands such as the velocity level can be changed on the fly. The controller also allows the user to change the coefficient of the stabilizing filter for optimum dynamic performance.

The control law has been implemented as a difference equation. It is a position control law with lead compensation, which eliminates the need for a tachometer. The user may change both the gain and the location of the lead compensation zero. This allows for adjustment of system stiffness and damping.

The mechanical specifications of the traverse are as follows:

Maximum travel: 3 m
Maximum load capacity: 5 kg
Straight line accuracy: 3 mm in 3 m
Positional accuracy: 1 mm over 3 m
Repeatability: 1 mm
Maximum speed: 150 mm/s

The data acquisition sequence is controlled via a software program by entering a set of commands governing the movement of the traverse (e.g., displacement and duration between moves, speed and acceleration) using the GALIL DMC-400 controller and data sampling procedure (e.g., sampling rate and duration, dynamic range/resolution, noise rejection and data validation, and data recording). A command file may be prepared with the operating parameters specified sequentially. Execution of the command file starts the data acquisition sequence for a single or multiple profiling cycles. Data are stored on the hard disk of the 386 PC with file identification of the recording time and date (e.g., 20OC1420.53 refers to a file recorded on October 20 at 14:20:53). The data files can later be transferred to floppies or cassette tapes for long-term storage.

3.2.6 Flow Facilities

For tests of the FODLDV in air, we used an air jet produced by fitting a nozzle 1 cm in diameter to the outlet of an ultrasonic humidifier (Gemtech Model AH-1501). Water droplets generated by the humidifier are excellent seeds for laser velocimeters. Liu and Bondurant (1988) provide a detailed

description of the facility and other peripherals designed to control the number density of water droplets in the airstream.

A series of tests was conducted in an oscillatory flow facility consisting of an air cylinder driven by a crank motor. The air cylinder is connected to a square vertical pipe (5.08 cm x 5.08 cm) with two optical windows made of microscope plate glass for the passage of the laser beam and viewing of the sampling volume. The pipe was filled with tap, Lake Washington, and Puget Sound water samples to determine the adequacy of seedings. The water column in the pipe undergoes an oscillatory motion when the crank motor is turned on as water is forced into and out of the air cylinder. The rotational speed of the motor controls the frequency, and therefore the speed, of the oscillation.

3.2.7 Miscellaneous Apparatus

Several apparatus were used in Phase II during the laboratory and field tests.

Nicolet Digital Oscilloscope

The Nicolet 4094 digital oscilloscope consists of three main components: the mainframe, the Model 4562 plug-in, and the XF-44/1 disk recorder. The mainframe includes a display memory, display screen, and various controls to manipulate the display-screen components. The controls feature horizontal and vertical expansion to a factor of 256, autocentering, a choice of XY and XT displays, a 16K word display memory that can be left intact or divided into halves or quarters, and multiple function abilities including arithmetic manipulations, electronic graticule, and pen recording outputs.

The Model 4562 plug-in includes two 12-bit, 500-nanosecond digitizers. Other features include two high-impedance differential amplifiers; a single 16K word memory; single-ended or differential amplifiers; positive, negative, or dual-slope triggering; normal trigger, pre-trigger, post-trigger, and delayed-trigger displays; a trigger view mode for setting up the triggering threshold; low-pass filtration; and sweep and point averaging.

The disk recorder transfers data onto the floppy diskette for storage. The stored data can be recalled at a later time for inspection on the screen. The diskette is divided into 20 individual records, each capable of storing either one (16K), two (8K), or four (4K) data groups. A set of 23 programs is available for statistical and waveform analysis of the signals stored on diskettes. For example, there are programs to estimate the maximum and minimum values, the rise time of a waveform, the area, and the average and root mean square (rms) values. Programs are also available for differentiation, integration, and inversion of the signals. The stored data can be transferred to the PC for further analysis and can also be displayed graphically.

Wind Sensors

For wind velocity measurement, we used two Gill propeller anemometers (Model 27106) manufactured by Young Company. The wind speed and direction may be derived from the combined

outputs of the two anemometers (Liu, 1991; Liu et al., 1985). Each anemometer is equipped with a generator and converter to provide a DC analog output proportional to the wind speed. The outputs are recorded via a second PC-based data acquisition system (DAS).

Wave Gauge

The wave height was measured with a thin-wire wave probe driven by a capacitance gauge. The probe is a stainless steel rod with a diameter of 0.32 cm. The output of the wave gauge was recorded with the second DAS.

Second Data Acquisition System

As mentioned above, in addition to the above-described 80368 PC-based DACS for the profiling FODLDV, a second PC-based DAS was used to record the wind and wave data. The A/D hardware consists of two PC plug-in boards with a resolution of 14 bits and a sampling rate of up to 1 MHz (Analogic Corporation, Fast-14-1-U series). These boards occupy two slots of an 80386 25-MHz, AT-compatible PC. There are a total of 12 channels, including 8 simultaneous sample and hold channels.

4. SOFTWARE FOR POST PROCESSING AND ANALYSIS

We used several scientific software packages such as the QUATTRO PRO spreadsheet by Borland, MATLAB by Math Works, Inc., SIGMAPLOT by Jandel Corporation, and QuickBASIC and C or QuickC by Microsoft. Microsoft C was used mainly in developing the programs for operating the FFT processor, for on-line data processing, for on-screen data display, and for data acquisition and recording. The other commercial software packages were used for post data processing, analysis, and graphic presentation. For example, MATLAB has a complete library of scientific routines for filtering, statistical, and spectral analysis, together with graphics. Most of the data analysis was therefore accomplished with MATLAB. Several subroutines, including the spike-removal program (the MMEDFILT), were developed by using the BASIC language to link data analysis programs furnished in the MATLAB library. However, for graphic representation of the experimental results, SIGMAPLOT is preferable due to its versatility.

Two programs were developed for post data processing. The source code for these programs is given in Appendix C in this volume. The first program, VALIDATA, decodes the raw data file and screens out the invalid data. Coding is incorporated in the time column, which consists of the sum of two integer numbers. The first number is either 0 or 128, depending on whether the data point is invalid or valid. The second number, expressed in units of the time sampling period 0.0005 s, corresponds to the fraction of time within each sampling window of the data sampling at which a Doppler burst is validated. For example, the sampling window is 0.005 s at a sampling rate of 200 Hz. The VALIDATA decodes the raw data file and outputs a time series that excludes all the invalid data points. The first column is the actual time in seconds at which a valid burst is registered, and the second column is the velocity components in centimeters per second.

The second program, the MMEDFILT, is the modified median filter developed for the removal of noise spikes. The MMEDFILT is programmed in a function form within the MATLAB program. There are three input parameters: the variable to be filtered, the number of neighboring points (odd) to be used in the median filter, and the speed jump defining the threshold of the noise spikes for removal. The output variable is a time series with the spikes replaced with the median values of their neighboring points.

For data analysis, programs such as the power spectrum and polynomial fitting are available in the MATLAB software package. These programs have been optimized for fast turnaround.

5. LABORATORY AND FIELD TESTS

The laboratory and field tests of the prototype profiling FODLDV are documented in this section. These tests were conducted to demonstrate the component/system performance and operating characteristics, respectively. From the combined test results, we determine the technical specifications and assess the range of field conditions under which the prototype operates most effectively.

5.1 LABORATORY TESTS

In the early stages of the Phase II research and development, many tests were conducted to select the optimum optronic components for the individual subsystems of the profiling FODLDV. Tests were also conducted to examine the performance of the subsystems. In this subsection, we report only those tests for the key subsystems such as the traverse and the FODLDV. These tests allowed us to determine the technical specifications and the range of operating environments of the FODLDV.

5.1.1 Traverse

The traverse was tested first without and then with the execution of the command files that control the data acquisition sequence (Section 3.2.4). The traverse may be operated by entering a single command or a sequence of commands that governs its movement via a PC through an RS-232 port. Upon completion of assembly, the traverse was tested in this mode to determine its performance characteristics. The test results demonstrate that the traverse moves very smoothly and meets all the requirements specified in Section 3.2.5. The system calibration of the traverse against a micrometer indicates that a 1-cm movement corresponds to 4244.14 optical encoder counts. This calibration factor was used in setting up the command files for velocity profiling.

To demonstrate the operational characteristics of the traverse in conjunction with the execution of the command file, tests were conducted in the laboratory and in the field. After many iterations, we have finally optimized the operational parameters (such as the rate of acceleration and deceleration of the motor) that are to be specified in the command file for trouble-free operation of the traverse. During field tests conducted in Luther Burbank Park on Mercer Island (which is located in Lake Washington in the Seattle area), the traverse worked well in autonomous mode--i.e., when controlled by the execution on the 80386 PC of several command files designed for different data acquisition sequences and procedures.

Based on the test results, the capability of the prototype profiling FODLDV may be greatly extended to encompass more sophisticated field measurement schemes. For example, it is relatively straightforward to implement the "yo-yoing" or "wave-following" mode of profiling. The yo-yoing mode may be achieved simply by modifying the command file so that the Doppler signals are processed and recorded simultaneously while the traverse is operating in a yo-yoing motion. The velocity data may then be corrected for by subtracting the motion of the traverse (recorded on one of the data channels). However, in implementing the wave-following mode, feedback of the wave displacement via the output of a highly repeatable wave gauge must be incorporated into the control circuitry.

5.1.2 FODLDV

As mentioned earlier, many tests were conducted on all optronic components during various stages of the Phase II development. Much effort has been made to optimize the performance of optronic components such as the diode laser, the beam splitter, the Bragg cells, the optical fibers and couplers, and the photodetector in terms of their efficiency/loss, polarization-preserving characteristics, stability, gain, and noise level (whichever are applicable to the components under consideration). In this subsection, we concentrate on the tests of the major components of the profiling FODLDV that were conducted using the completed assembly. Most of the tests were conducted in the air jet seeded with water droplets and in the oscillatory flow facility (Section 3.2.6); the former and the latter were used for qualitative and quantitative assessment of the instruments, respectively. Other tests were conducted in the wave tank at Oregon State University and on a concrete boat dock in Luther Burbank Park on Mercer Island (which is located in Lake Washington in the Seattle area).

Digital FFT Processor

A series of tests to assess the performance of the FFT processor was conducted upon its completion in the wave tank of Oregon State University during the SUPERTANK experiment (Agrawal et al., 1991). During that experiment, a previous-generation FOLDV consisting of a 3.8-cm diameter fiber-optic probe equipped with a 10-mW He-Ne laser and an analog FFT processor (Agrawal, 1984) on which the new one was based was used to study the transport of sands in a mechanical wave field. To evaluate the performance of the digital FFT processor relative to that of its established analog counterpart, output signals from the FOLDV were connected in parallel to both instruments. Comparison of test results obtained using the same FOLDV allowed us to quantify the improvement in performance that is attributable to the digital processor, which was specifically developed to replace its analog counterpart.

The comparison was conducted by operating the two processors under approximately the same conditions; note that the comparison thus did not take full advantage of the new features of the digital processor by operating it with the optimized settings. For example, the sampling rates were 25 and 50 Hz for the analog and digital processors. The threshold parameters were set to SL = 58 and SV = 18 instead of the optimum values of SL = 20 and SV = 15, excluding many relatively weak burst signals. In addition, the TS 0 FFT window of the digital processor with the maximum velocity range of 3.2 m/s and the lowest resolution of 1.25 cm/s was selected.

Figure 8 illustrates the comparison of the two time series derived from the two instruments. Figures 8(a) and 8(b) show the time series with noise spikes of greater than 5 cm/s removed using the MMEDFILT program. The time series shows that the dominant wave has a period of 8 s. There are, however, higher harmonics in the mechanical wave train that do not appear to be completely resolved at the sampling rate of 25 or 50 Hz as a result of aliasing (see Figures 9 and 10). The overall comparison shows very good agreement. The frequency of occurrence of the noise spikes in the raw signals is about the same in both cases. The time series measured with the digital processor (solid) contains more detail

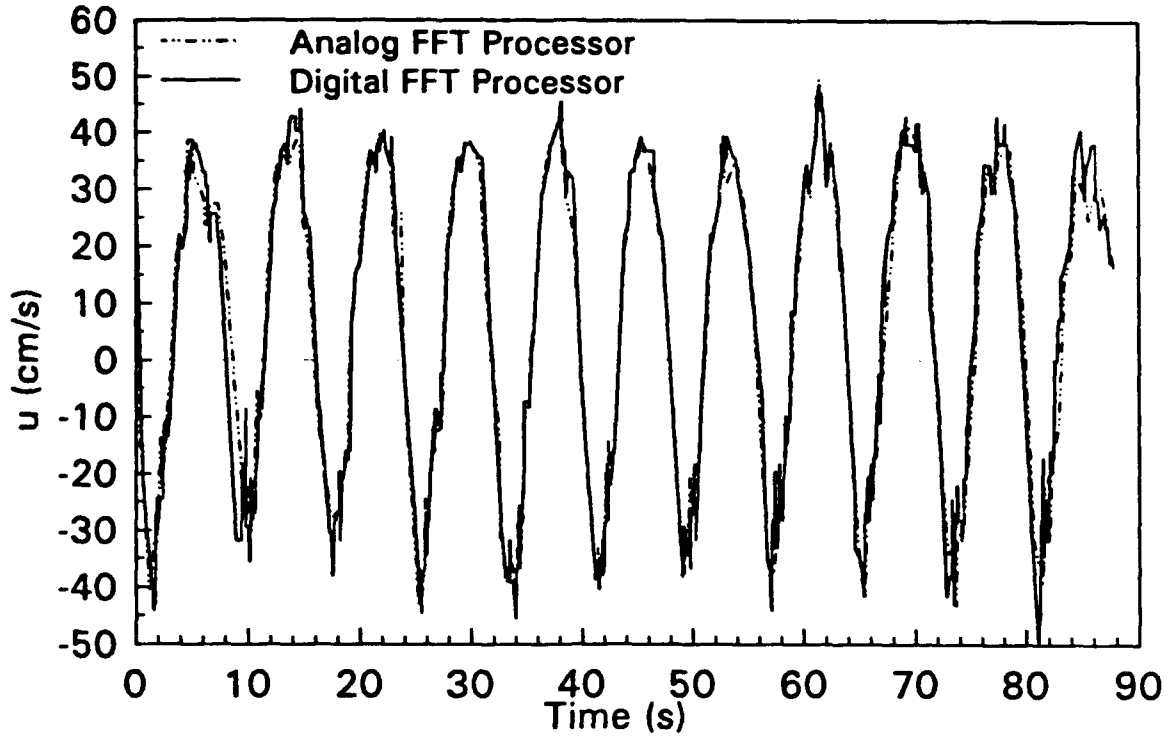

a. 90 seconds of data

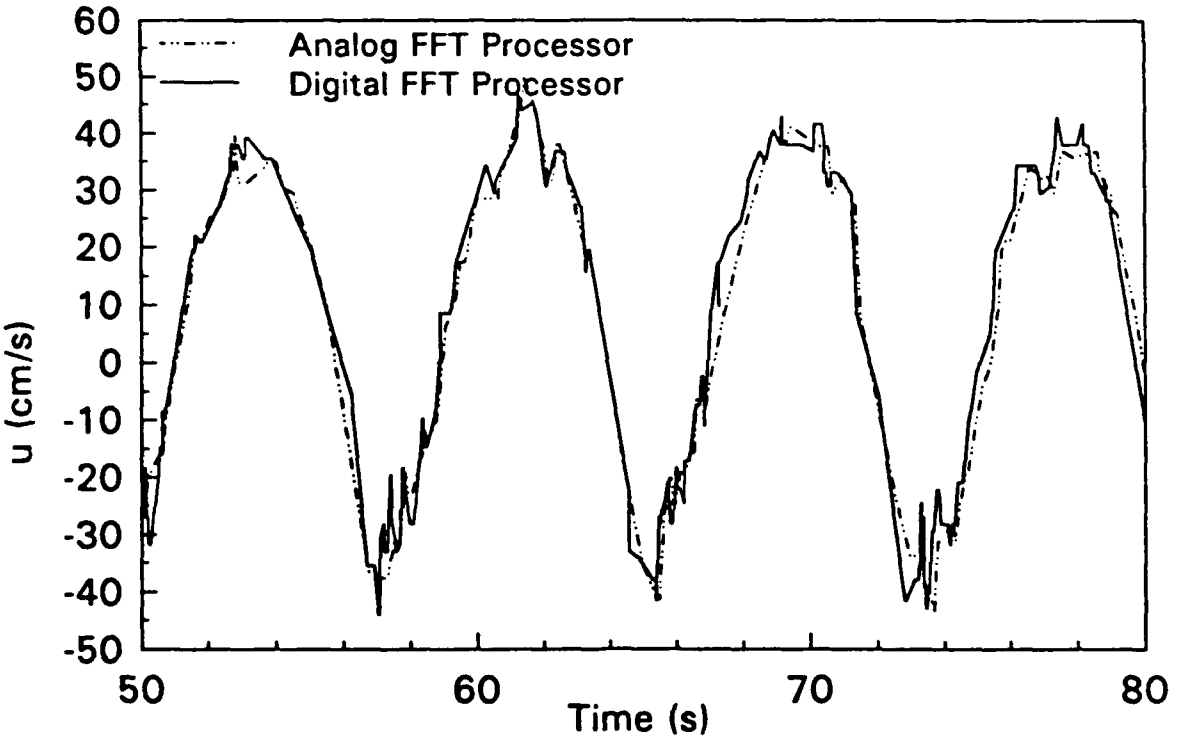

b. Expanded time scale

Figure 8. Velocity Time Series Measured with the Analog and Digital FFT Processors

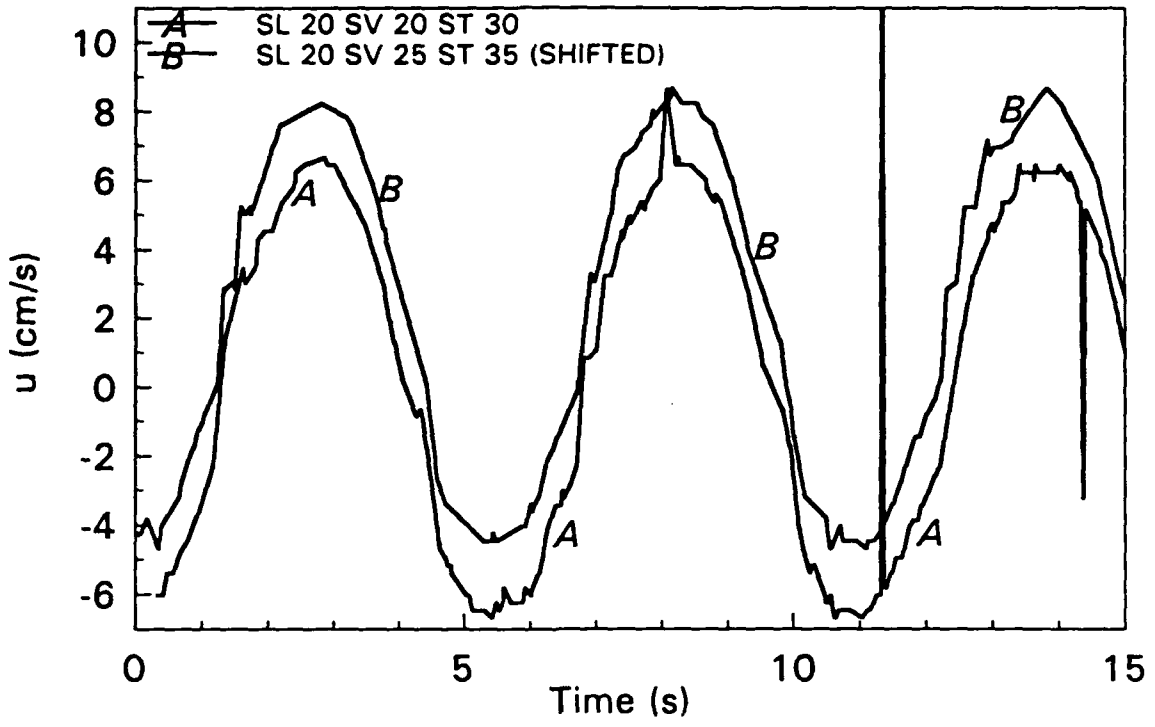

Figure 9. Time Series of an Oscillatory Flow Using an APD

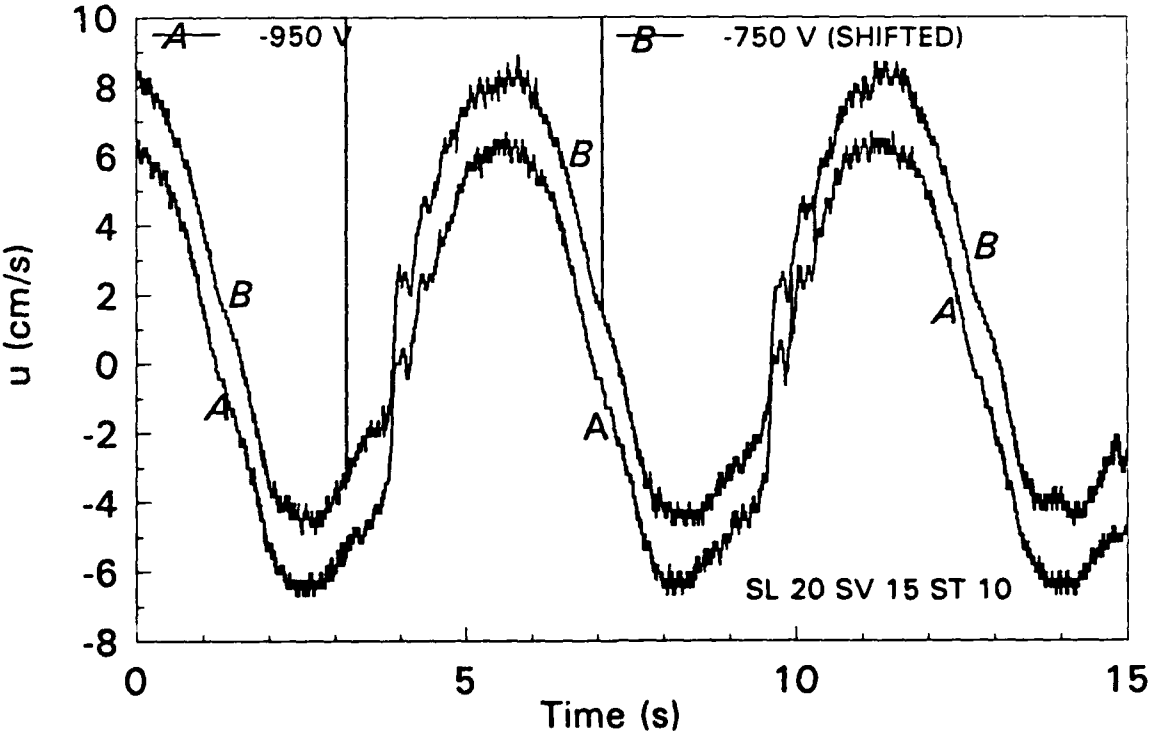

Figure 10. Time Series of an Oscillatory Flow Using a PMT

than that measured with the analog processor (dash-dot-dot); this is reflected by a higher data rate for the former (13.4%) than for the latter (9.6%) with a ratio of 1.4. The relatively low data rate, which is inherent due to the large size sand particles with diameters larger than that of the focal volume, results in missing some of the detail of the high harmonics. On the other hand, the FOLDV had a net laser power of about 2 mW at 632 nm for all three beams, and the backscattered light from small particles was simply too weak to be distinguishable from the noise in the systems. A combination of higher laser power, optimum processor threshold settings, and intelligent processing algorithms will be required to improve the signal quality.

The above comparison has verified that the digital FFT processor functions properly as designed. We anticipate that improvement in the signal quality may be achieved by using the optimum settings for the experiment conducted for comparison. For example, the maximum velocity amplitude measured in the wave train is less than 0.5 cm/s. It is preferable to select the second FFT window, TS 1, with a velocity range of 1.6 m/s and a resolution of 0.62 cm/s (for the FOLDV), to double the resolution in the measurements. Lowering the values of the threshold settings to SV = 12 and SL = 20 would validate more weak bursts and thus increase the data rate; this would also result in more noise spikes, but they can be effectively removed using the MMEDFILT during post processing. In measuring the detail of the high harmonics riding on the wave train, selecting the maximum data rate of 200 Hz would result in a higher data rate and a reduction in the aliasing problem for the high frequency components. Furthermore, the FODLDV has a net laser power of 24 mW at 830 nm, which is ten times that of the FOLDV. The tenfold laser power would significantly boost the intensity of the backscattered light from small particles and therefore increase the data rate.

Photodetector Effects

One of the test series was conducted to compare the performance of the APD and PMTs. Velocity measurements were conducted using Channel 1 (1 MHz Bragg-shifted) of the FODLDV in the oscillatory flow facility filled with sample water from Lake Washington. Figure 9 presents two velocity time series, A and B, measured with the APD for two different sets of threshold or validation parameters: SL = 20/20, SV = 20/25 and ST = 30/35. For clarity in comparing the two series on the same graph, we shifted series B in time and upward by 2 cm/s. Experiments were conducted by selecting the fourth FFT window (TS 3) with a maximum frequency of 62.5 kHz or velocity of 55.1 cm/s. The corresponding bin width is therefore 244.1 Hz or 2.2 mm/s. The mixing frequency for Channel 1 is 1.031 MHz, which places the zero velocity at 31 kHz. The sampling rate, SR, was selected to be 200 Hz. The data rates, as calculated using the ratio of the validated to the total measured data points, are 7% and 5%, respectively, for the two series. The increase in the data rate with lower values of the validation parameters is evident. The measured amplitude and period were approximately 6.3 cm/s and 5.5 s. For a 5.5-s wave sampled at 200 Hz with a 100% data rate, there should be 1100 data points for each wave cycle, and the measurements should be more than adequate to describe the velocity profile in great detail. In reality, Figure 9 shows that the data rate was so low that the measurements barely tracked the velocity profiles of the dominant wave motion and failed to reproduce the presence of the high harmonics. For series A, with

relatively low values of the validation parameters, noise was being triggered and validated occasionally, contaminating the time series in the form of large-amplitude spikes whose width rarely exceeded one sampling time period. However, such sharp spikes, which are characteristic of LDV signals when the threshold is set too low, can be effectively removed using the MMEDFILT developed in the present investigation based on the principle of order statistics (Gallagher and Wise, 1981) as shall be demonstrated later.

In comparison, Figure 10 illustrates the same velocity time series measured with the FODLDV using the R636 PMT driven by a high voltage of -950 V (A) and -750 V (B). The same sampling rate of 200 Hz was used with relatively low values of the validation parameters (SL = 20, SV = 15 and ST = 10). The data rate increased 15-fold from an average of 6% to 91%. As a result, the measurements now track the velocity profile in great detail. Furthermore, no noise spike appears in the 30-s period. The significant reduction in the frequency occurrence of the noise spikes also indicates a greater improvement in the SNR, which is primarily responsible for the increase in the data rate. For the optimum sampling condition discussed above, the values of the validation parameters may be set even lower such that noise spikes appear occasionally.

Careful examination of the velocity time series shows the presence of high-frequency components at several fixed phases of the oscillatory velocity time series, particularly in the troughs and crests. These components, which are quite repeatable, were not detected with the use of the APD due to the low SNR. They are generated by the driving mechanism and by the restriction in the small tube connecting the cylinder and the square tube. Their amplitudes are close to the resolution or bin width of the TS 3 FFT window (i.e., 2.2 mm/s). They may be better resolved by selecting an FFT window with a narrower velocity range or finer resolution (e.g., TS 4 or 5). We will look into this aspect shortly.

In a condition in which the PMT was driven at -750 V, with a gain much higher than that achieved with the APD, the raw signals displayed on the oscilloscope have shown that most of the large Doppler bursts are just below the saturation level of ± 2.5 V. Further increasing the magnitude of the supply voltage to -950 V results in exceeding the saturation level for most of the large bursts. The saturated Doppler signals introduce sidebands with lower spectral peaks than that of the Doppler frequency as can be observed on the near-real-time screen display of the spectrum distribution. Because the FFT processor selects only the dominant peak with the highest spectral density corresponding to that of the Doppler frequency, no error is introduced even in the presence of many higher harmonics. In fact, there is a general improvement in the validation rate for the PMT operating at high gain so that signals from small bursts may also exceed the noise level and be detected and validated.

Figure 11 illustrates two typical sets of medium-strength Doppler signals measured with the R636 PMT operating at -900 V and with the FFT window set to TS 3 (i.e., with the raw signals mixed at 1.031 MHz). The measurements were conducted in the oscillatory flow facility filled with water sampled from Lake Washington. Figures 11(a) and 11(b) correspond to Doppler bursts generated by a single particle and two particles (one immediately after the other) moving through the focal volume of the FODLDV. Both signals are of extremely high quality and SNR, resulting in validated velocity data.

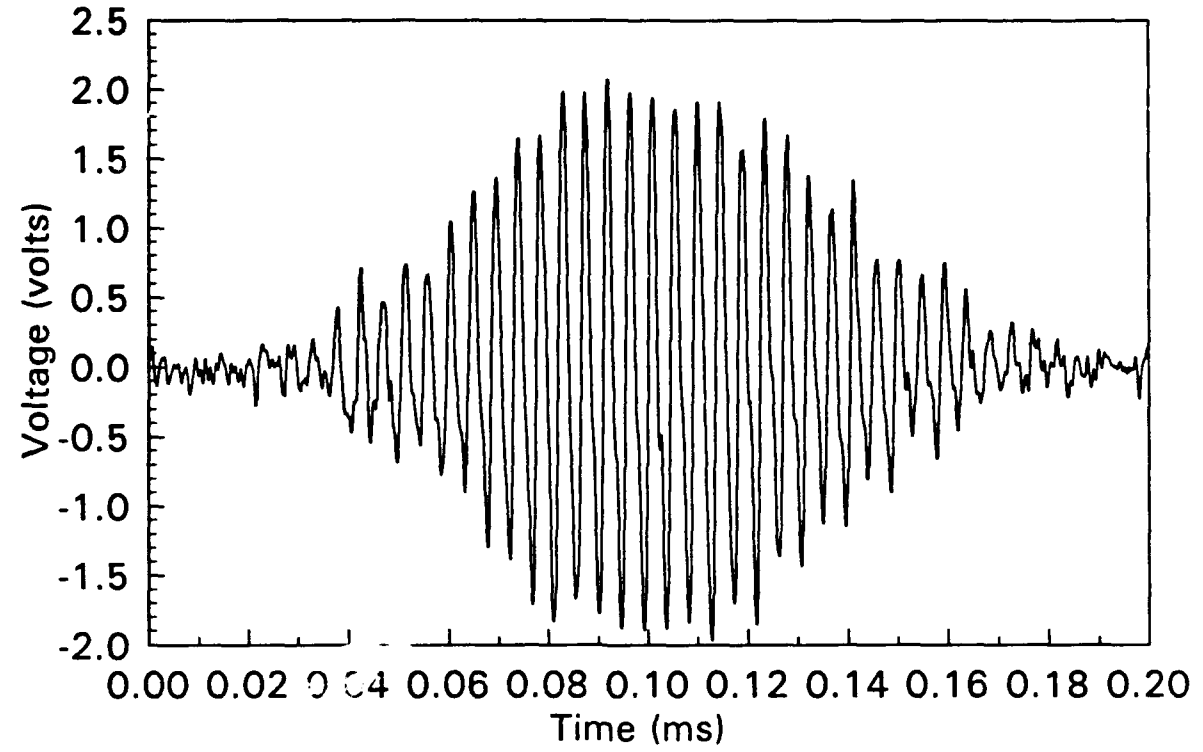

a. Single particle

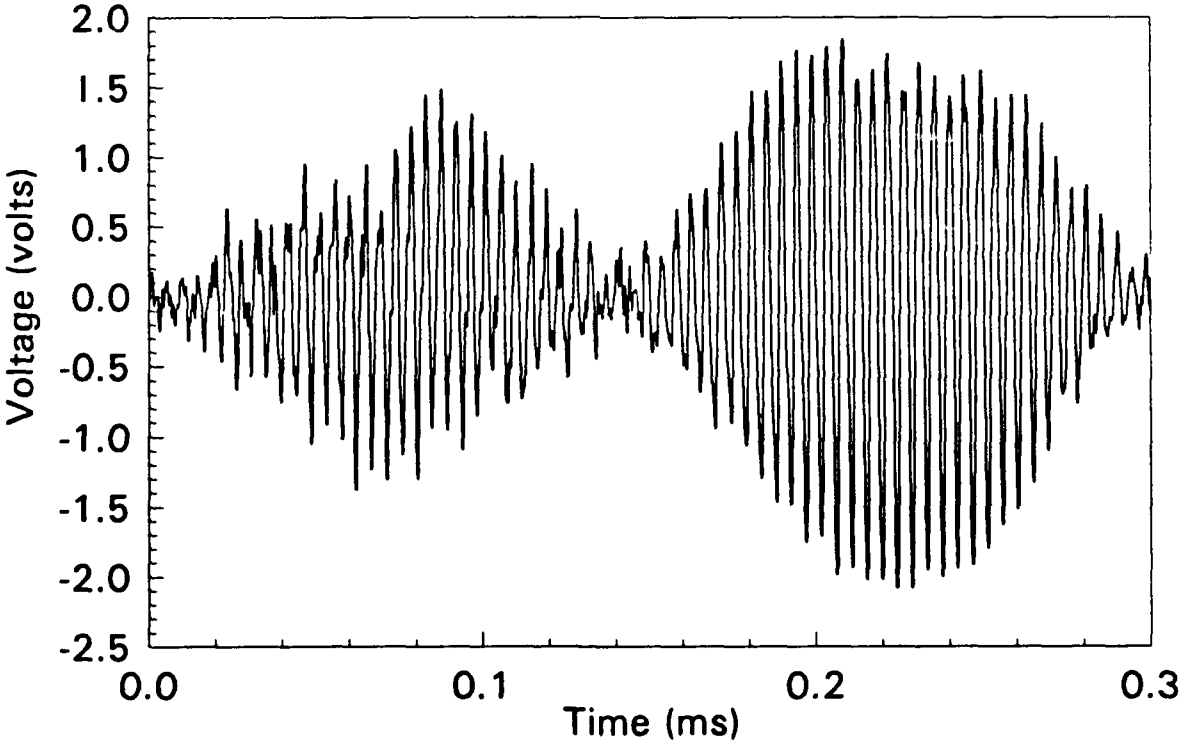

b. Two particles, one following the other

Figure 11. Typical Doppler Burst Signals

There are a total of about 30 fringes in each burst. The number of fringes with peak intensity above the e^{-2} level is approximately 20, which is consistent with the estimated number of 18 (Section 3.2.1) based on the geometry of the laser beams.

Velocity Range and Resolution

To demonstrate the optimum selection of velocity range or resolution, we compare in Figure 12 three velocity profiles--A, B, and C--measured with the use of three FFT windows: TS 3, 4, and 6. These windows correspond to the Doppler frequency/velocity range or resolution of (62.5 kHz/55.1 cm/s, 244.1 Hz/2.2 mm/s), (31.25 kHz/27.5 cm/s, 122.1 Hz/1.1 mm/s) and (7.81 kHz/6.9 cm/s, 30.5 Hz/0.27 mm/s), respectively, with resolution ratios 1, 2, and 8 (see Table 1). The sampling rates used for the measurements were 200, 100, and 30 Hz as the maximum sampling rate decreases with the increase in the resolution. To ensure that the maximum velocity does not exceed the velocity range of window TS 6, we reduced the oscillatory period to 12.5 s. Only the crest of the velocity profiles are plotted in the figure to show the details of the high-frequency wavelets.

The lack of resolution for TS 3 is evident from the figure as the low-amplitude wavelengths are barely resolved; the height of the stepwise feature corresponds to the resolution of 2.2 mm/s. This situation improves progressively as we change from TS 3 to TS 4 and then TS 6. On the other hand, the relatively low sampling rate of 30 Hz for TS 6 results in partially missing details of the high-frequency wavelets due to aliasing. When both velocity range or resolution and the sampling rate are considered for the measurement of the oscillatory motion of interest, the optimum FFT window is therefore TS 5. It should be pointed out that sub-bin resolution to a factor of at least a half through interpolation of the spectral profile calculated in the FFT processor to determine more precisely the spectral peak is achievable via software manipulation within the DSP.

Particle Concentration Effects

One of the motivations for developing the profiling FODLDV is to shorten the optical path to minimize blockage problems in waters with high turbidity, such as in an estuary. To simulate various particle concentrations, small, nearly spherical polystyrene particles with an average diameter of 0.5 mm and a specific gravity of 1.03 were added to the oscillatory flow facility, which has a total capacity of four liters. These particles are not always well separated in suspensions; large lumps tend to form as a result of several particles clinging together. This was often observed through the glass windows.

Figure 13 illustrates four velocity profiles, A through D, measured with the TS 6 setting for volume ratios 0, 1.3, 2.5 and 5%. Note that this experimental setup does not represent the worst scenario as half of the optical path was in air and the other half was in water inside the square tube of the facility. Comparison of the velocity profiles has shown little difference for volume ratios up to 1.3%. Serious degradation in the velocity profiles is observed for volume ratios of 2.5% and higher. The degradation takes the form of the frequent appearance of velocity anomalies with speeds lower or higher than the local fluid speed at the high or low speed cycle of the oscillation as observed in profiles C and D. These

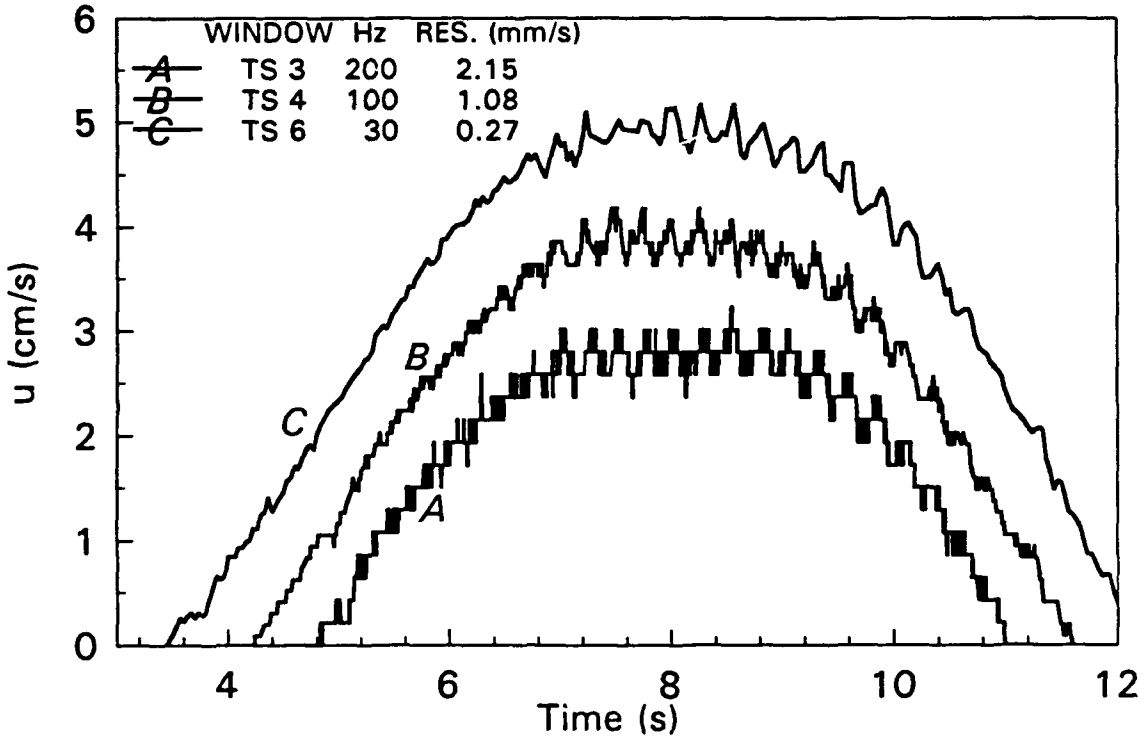

Figure 12. Optimum Selection of Velocity Range or Resolution

Table 1. Conversion of Frequency and Velocity Parameters

FFT Windows	Time Sample	Burst Digitization Rate	Maximum Doppler Frequency	Frequency Resolution	Maximum Velocity*	Velocity Resolution**
1	0	1.0 MHz	500 kHz	1.953 kHz	4.41 m/s	1.72 cm/s
2	1	500 kHz	250 kHz	976.6 Hz	2.20 m/s	0.86 cm/s
3	2	250 kHz	125 kHz	488.3 Hz	1.10 m/s	0.43 cm/s
4	3	125 kHz	62.5 kHz	244.1 Hz	55.1 cm/s	0.21 cm/s
5	4	62.5 kHz	31.25 kHz	122.1 Hz	27.5 cm/s	1.07 mm/s
6	5	31.25 kHz	15.63 kHz	61.04 Hz	13.8 cm/s	0.54 mm/s
7	6	15.63 kHz	7.813 kHz	30.52 Hz	6.88 cm/s	0.27 mm/s
8	7	7.813 kHz	3.906 kHz	15.26 Hz	3.44 cm/s	0.13 mm/s

*The range is plus or minus half of the maximum value if the local oscillator is set to the midpoint of the maximum Doppler frequency

**Based on a calibration of 1.135 kHz/(cm/s)

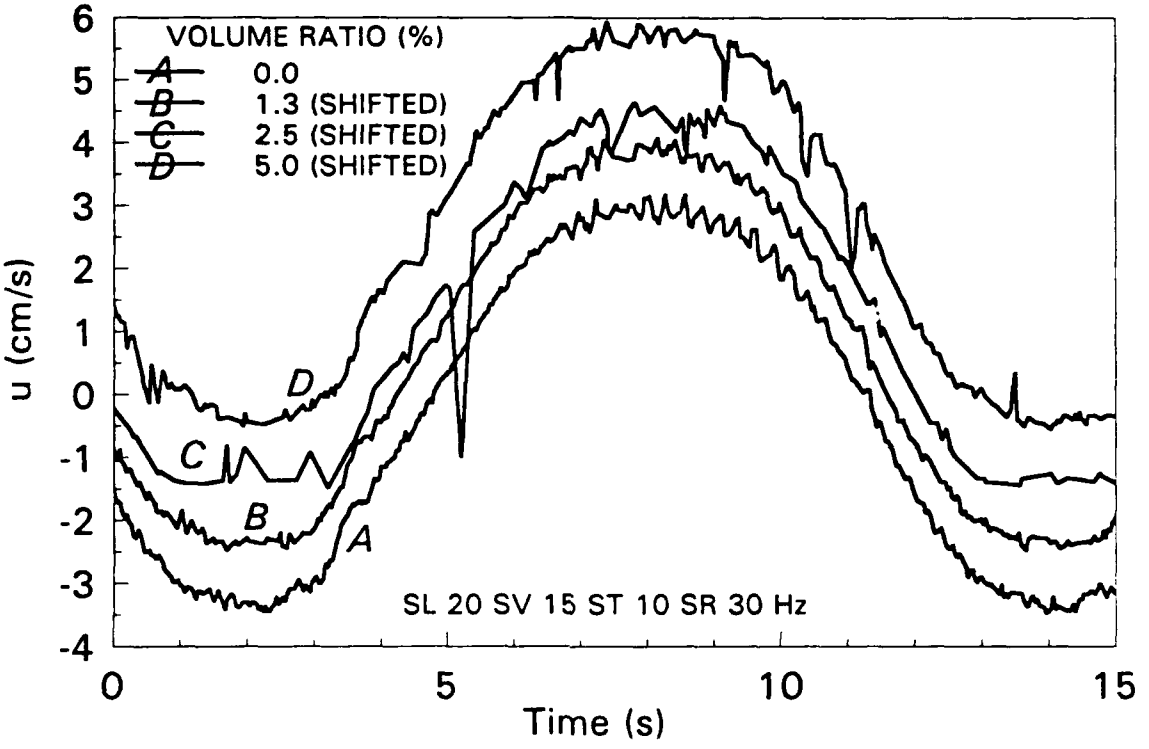

Figure 13. Effects of Particle Volume Ratio on Data Rates

anomalies have much lower amplitudes (most of them less than 1 cm/s) than the noise spikes (greater than 5 cm/s as defined) that are removed by the MMEDFILT. In most cases, the anomalies correspond to the passage of large particles or lumps through the focal volume. The relatively large drag force on the lumps results in a considerable lag between the speeds of the lumps and of the fluid whereas small particles are capable of following the low frequency oscillatory motion closely. Whether there is a lag between the particle and fluid motion depends on the velocity relaxation of the particles (Pai, 1977). It is therefore anticipated that the amplitude of the anomalies increases with increasing oscillatory frequency of the flow. The above interpretation is consistent with the characteristics of the anomalies that appeared in the measured velocity profiles in water with a high particle concentration. The capability of measuring the velocity lag between the particle and fluid velocity in an oscillatory flow with the FODLDV suggests an excellent method for studying particle dynamics in fluids.

Filter for Noise-Spike Removal

In the course of developing an earlier DLDV (Liu and Bondurant, 1988), the authors established an acceleration criterion for identifying the spikes to be removed in post analysis. In essence, a noise spike is defined and removed provided the product of its amplitude and the sampling rate or the equivalent acceleration exceeds the maximum acceleration that can be sustained physically by the flow under investigation. The computer program MMEDFILT that was developed during Phase II combines this acceleration criterion and a median filter (Gallagher and Wise, 1981). The median filter has several advantages over a low-pass filter in that the former is invariant for a monotonically decreasing and increasing time series and in that it removes spikes yet preserves sharp edges. With the incorporation of the acceleration criterion, the MMEDFILT is invariant for a time series in the absence of noise spikes. In other words, the passage of a spike-free time series through the filter preserves the time series exactly. The MMEDFILT is therefore very different from a median filter or a low-pass filter. Consider a time series, v(i), with occasional noise spikes satisfying the acceleration criterion, where i is the index from 1 to the total number of data points. When a noise spike is encountered at *i*, the program replaces the spike with the median value of the neighboring 2N+1 data points v(i) through v(i+2N+1) where N is an integer. All isolated noise spikes will be removed with a single pass of the time series through a three-point MMEDFILT. A single passage of a five-point MMEDFILT removes spikes appearing consecutively in the times series, although the optimum threshold criterion excludes even a low probability of such consecutive appearance.

In Figure 14, we compare the original (A) and the filtered (B) time series with a period of 5.5 s and a velocity amplitude of 7 cm/s. As seen from Figure 14(a), there are twelve spikes in the 15-s-long time series, with a frequency of appearance of less than 0.5% of the data rate. The settings of the validation parameters are somewhat higher than the optimum settings determined using the acceleration criterion and were chosen arbitrarily to demonstrate the effectiveness of the MMEDFILT for spike removal. The validated signal A corresponds to that processed once by removing all the invalidated data points in the raw signals, whereas B is the data filtered through the MMEDFILT program with the acceleration threshold set at 3 m/s^2 or 0.3 g. For a 5.5-s wave with an amplitude of 7 cm/s, the maximum acceleration

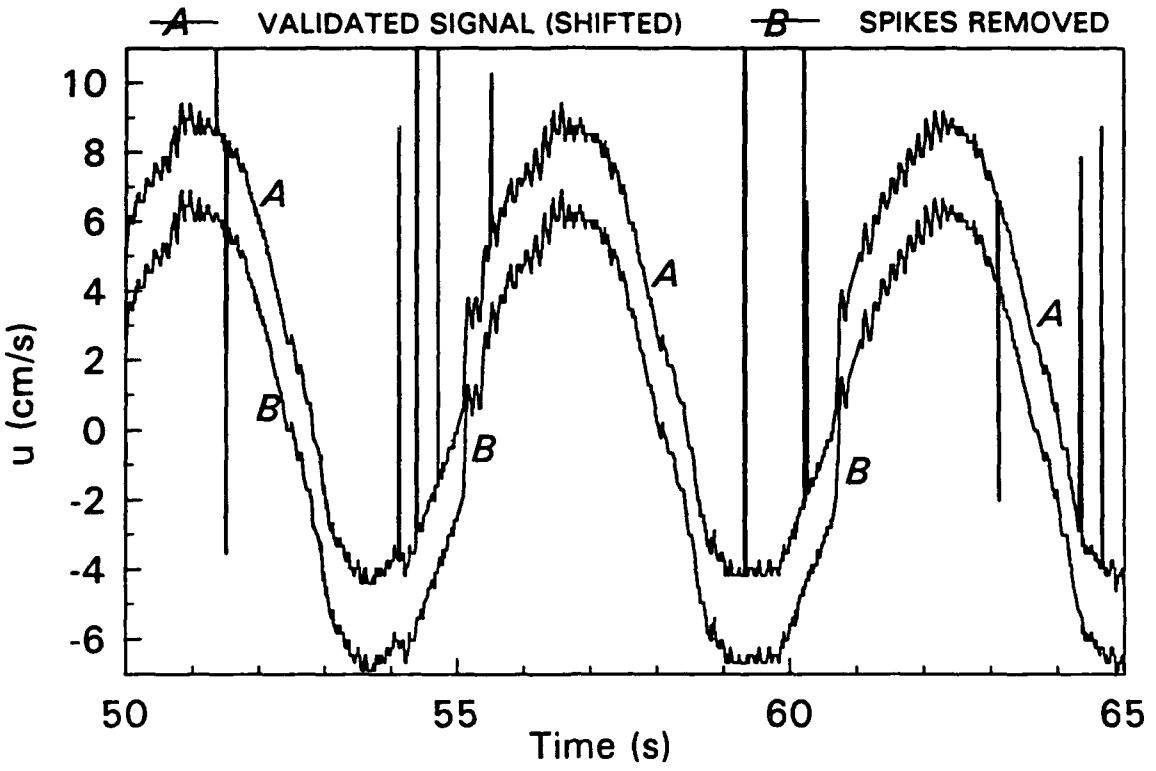

a. 15 s of data

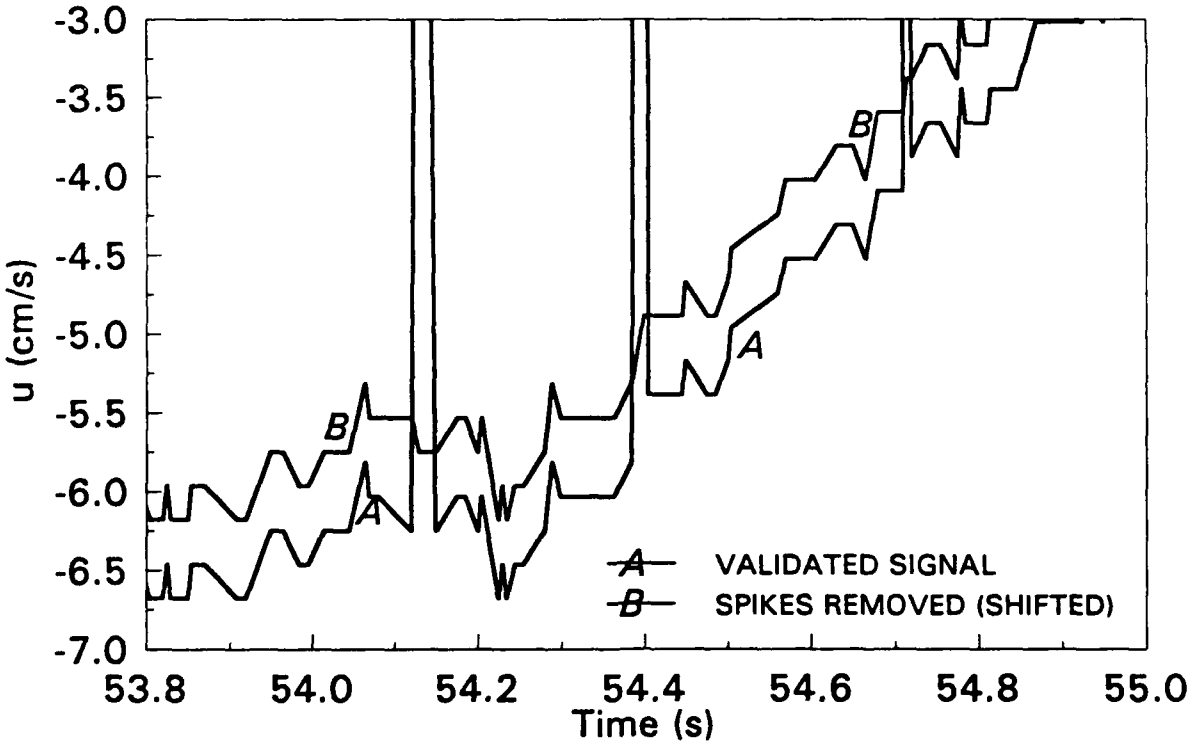

b. Invariance of MMEDFILT with multiple passage

Figure 14. Comparison of Unfiltered and Spike-Removed (MMEDFILT) Velocity Time Series

without breaking is 0.08 m/s^2 or 0.008 g. The noise spikes are completely removed by passing A through the MMEDFILT once using an acceleration criterion of 0.5 g, as shown in B. Note that all the detail of A is preserved in B except in the immediate neighborhood of the spikes. Figure 14(b) displays the same two signals greatly expanded in the time and velocity axes to further examine the result of the spike removal program. It is clearly demonstrated that the modifications are indeed very localized as discussed.

At present, one of the most difficult aspects of LDV measurement is to determine the optimum threshold setting; it is still a "black art" that requires extensive experience rather than a science. The best recommendation offered by LDV manufacturers has simply been "master the technique by trial and error." This difficulty in determining the optimum threshold setting has been one of the main obstacles to wide acceptance of the LDV, even within the research community, since its first introduction nearly three decades ago (Durst et al., 1976). The successful implementation of the MMEDFILT for spike removal has led to refinement in defining the optimum threshold of the validation parameters, which will most definitely accelerate acceptance of the LDV as a research and industrial tool for velocity measurements.

To find the optimum threshold setting, one simply increases the threshold to the point at which noise spikes appear occasionally; this is done with the help of the real-time histogram screen display (Section 3.2.4). The optimum frequency of spike appearance should generally be no more than 1% to 2% of the data rate depending on the flow conditions and the accuracy requirements. The percentage tolerance is higher in laminar than in turbulent flows as the median filter is more reliable in recovering the original time series with monotonically decreasing or increasing rather than fluctuating values in the neighborhood of the spikes. As a rule of thumb, consecutive appearances of spikes should be avoided even though a five-point median filter is capable of removing these spikes. In practice, the application of the MMEDFILT is no worse than the algorithm of assigning the previous value of the time series for an invalidated velocity point. With the low percentage of spike appearances, as recommended, it would not be expected that the MMEDFILT would change the statistics and spectral characteristics of the otherwise spike-free measurements. Yet, lowering of the threshold values allows weak bursts with marginal SNRs to be validated, assuring the optimum setting of the validation parameters to obtain the maximum data rates that are essential for high degrees of fidelity.

To further demonstrate the effectiveness of the MMEDFILT, we present in Figure 15 the power spectra of the time series of the oscillatory velocity with a period of 5 s and an amplitude of 7 cm/s similar to that shown in Figure 14. The measurement was conducted using the TS 4 window with a resolution of 1.1 mm/s. The spectrum was calculated with an 2048-point FFT using a Hanning window for a record length of 250 s and a sampling rate of 100 Hz. The frequency of spike appearance for this case is 3.0%, which is higher than the recommended 2% limit. The abscissa and ordinate are the frequency in Hz and the spectral density of the oscillatory velocity in cm^2/s. Curve A is the power spectrum of the validated raw signal without the removal of the spikes. The spectrum shows a spectral peak at 0.2 Hz which corresponds to the dominant oscillatory motion. A bank of higher harmonics with a slight decrease in the peak spectral density with increasing frequency is observed up to approximately

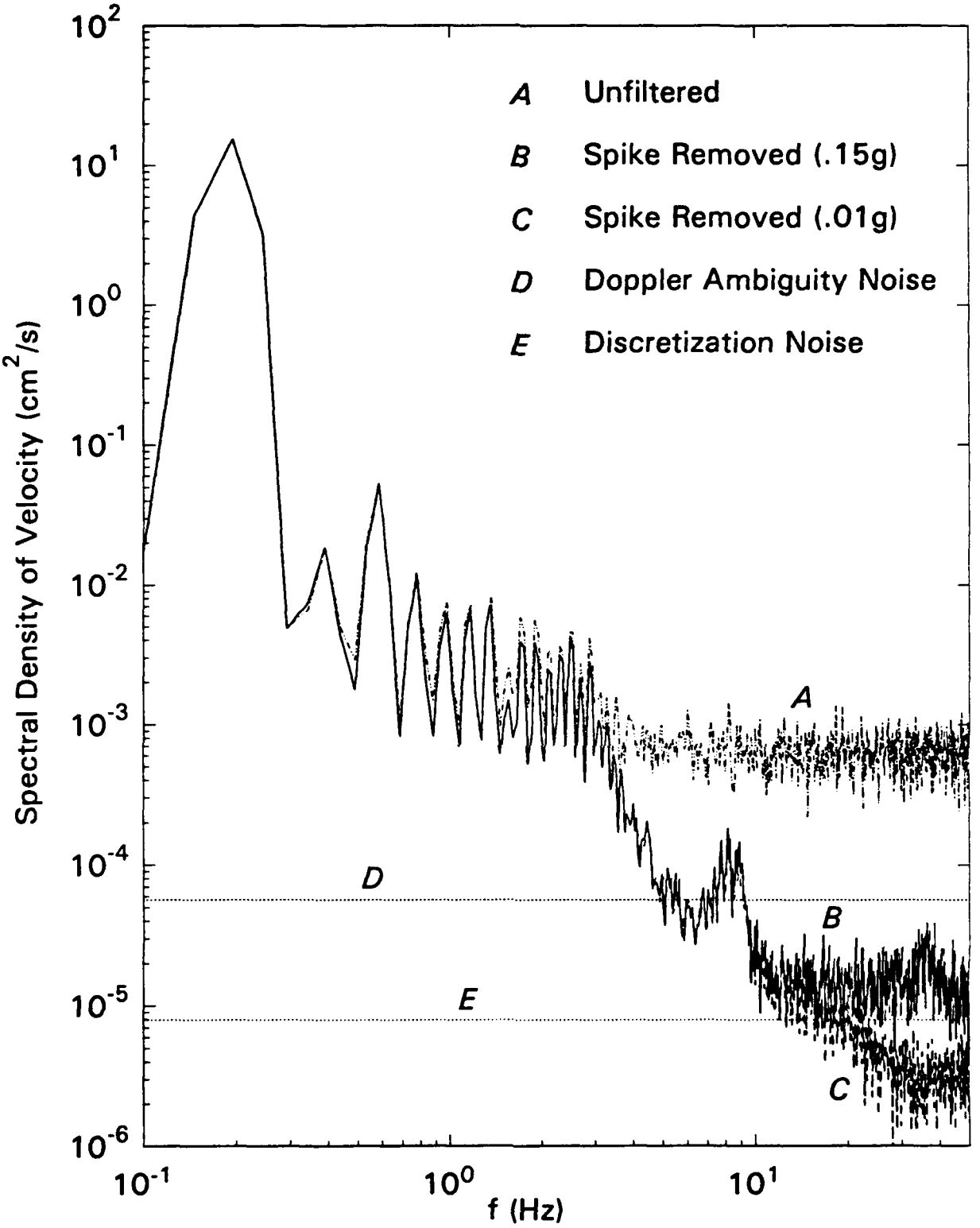

Figure 15. Comparison of Velocity Power Spectra

3 Hz. These correspond to the high-frequency wavelets riding on the oscillatory flow as seen in Figures 12 and 14(a). The presence of the noise spikes contaminates the spectrum severely for frequencies greater than approximately 4 Hz, and the noise spectrum appears to be white up to 50 Hz. For a 5-s velocity oscillation with an amplitude of 7 cm/s, the maximum acceleration is $2\pi(0.2)7 = 8.8$ cm/s^2 or 0.009 g. With the spikes removed using the acceleration criterion of 0.15 g or a velocity jump of 1.5 cm/s sampling at 100 Hz, the velocity spectrum (Curve B) is essentially unchanged up to about 3 Hz and begins to drop off rapidly beyond that frequency. There is a small hump at approximately 8 Hz, and the spectrum levels off beyond 10 Hz. The ratio of the spectral densities at which spectrum A and B level off is about 50 or one-and-a-half decades. Most importantly, the MMEDFILT allows the recovery of physical features in the spectral domain which would otherwise be buried into the noise without the removal of the spikes or simply lost if the validation parameters were set too high to avoid the spikes.

Also shown in the figure are the estimated Doppler-ambiguity broadening of 5.7×10^{-4} cm^2/s (D) as given by George and Lumley (1973) for laminar flows and the discretization noise 1/12 (resolution)2/bandwidth = 8×10^{-5} cm^2/s. The observation that the noise level of the spike-removed velocity spectrum B is lower than the ambiguity broadening D is a pleasant surprise. Evidently, the assumption of random entry of multiple particles, each scattering the same amount of light moving through the focal volume, that is used in deriving the Doppler-ambiguity broadening is too conservative in this case. First, the tap or Lake Washington water used in the oscillatory flow facility was very clean (this is especially true of the tap water). The probability of multiple particles entering the focal volume at any one time may be low. Second, each particle entering the probe volume has different scattering characteristics. The strongest scatter is expected to dominate the scattered signal collected at the PMT. As a result, the above scenario is likely to reduce the Doppler-ambiguity broadening as predicted by George and Lumley (1973).

For a specific experimental condition, the FODLDV can be either Doppler-ambiguity or discretization-noise limited. In most cases, the ambiguity noise level, D, is higher than the discretization noise level, E. An optimization of the optronic design that may be considered is to match E with D. For the present situation discussed above, D appears to be overestimated using the formula derived by George and Lumley (1973); however, the actual value of D is not known.

Let's assume that the actual D is the same as E. Figure 15 shows that the noise floor of spectrum B is higher than E. We may then lower the threshold of the noise spikes below 0.15 g to match the noise floor of the spectrum with that of E. Any information with spectral density below the level of E is therefore contaminated. Lowering the spectral floor below E by further reducing the threshold of the noise spikes does not result in recovery of the lost information and introduces a risk of removing spectral components at low frequencies. In other words, the threshold of 0.01 g is definitely below the optimum value, so that part of the real signal might have also been removed by the MMEDFILT. Additional runs of the time series through the MMEDFILT have demonstrated that the optimum threshold is 0.1 g according to the above criterion.

5.2 FIELD TESTS

Field tests were conducted to demonstrate the operating characteristics of the prototype under typical field conditions. Based on the test results, we further optimized the logistics and operating procedures of the profiling FODLDV. Modifications to the optronics were also made to improve the performance of the FODLDV.

A series of field tests was conducted at Luther Burbank Park, Mercer Island, Washington. The park has several concrete boat docks on a solid foundation extending as much as 50 m from the shore into Lake Washington. The docks serve as an ideal stationary platform for testing the profiling FODLDV with insignificant influence from the shore topography. The water depth at the end of the dock is more than 16 m deep. The site is a very good one except that the water is relatively clean, containing few small particles to act as tracers.

The series of tests was conducted on September 26, 1991. During the tests, the profiling traverse and the FODLDV were mounted on the end of the longest dock, with the probe head oriented to measure one of the horizontal components aligned close to that of the mean wind speed. We also set up a two-component propeller anemometer and a vane anemometer on a portable meteorological tower (6 m above the water surface) and a capacitance wave gauge to monitor the wind and wave conditions. Other instruments included a hand-held wind speed indicator, a compass, and an instrument to read the wet bulb temperature. The wind and wave data were recorded on the second PC based DAS.

For each run, the test procedure is entered into a command file consisting of a sequence of commands that set up relevant parameters for the FFT processor, the traverse, and data acquisition and recording. The traverse was tested only in the stop-and-sample mode. The profiling positions were programmed to move downward according to a logarithmic scale.

Several runs were conducted, and the system functioned well as designed. We have tested the logistics and the profiling capability extensively and were satisfied with this aspect of the operation. During the field experiment, the APD was used as the photodetector. The combination of low wind and low current situations on the test date and the insufficient sensitivity of the APD (see Section 5.1.2) resulted in a very poor SNR and an extremely low data rate; meaningful interpretation of the data was therefore not possible. The poor performance of the APD led to the replacement of the APD with a PMT, which significantly improved the performance of the FODLDV (see Section 5.1.2).

6. SUMMARY

A prototype field-worthy, two-velocity-component, fiber-optic diode laser Doppler velocimeter (FODLDV), with a maximum profiling range of 3 m, has been successfully developed, evaluated, and tested in the laboratory and in the field. The profiling FODLDV, operating in the backscattered mode, was designed to be mounted on a stationary platform for deployment in coastal waters; it is also suitable for use in other water bodies such as lakes, rivers, and estuaries. The traverse was designed to operate in move-stop-and-sample mode but may be modified to operate in "yo-yoing" or "wave-following" mode. The combination of medium laser power, a short optical path, and advanced signal processing is the key for deployment of the FODLDV in both clean and turbid waters.

Special features allowing on-line, real-time display of the histogram and near-real-time display of the spectral distribution of the data on the monitor were implemented to help simplify and optimize the setup of the digital FFT processor. For post data analysis, the MMEDFILT algorithm was developed by combining a median filter and an acceleration criterion for effective removal of noise spikes inherent in laser anemometry. The successful implementation of the MMEDFILT allows considerable lowering of the thresholds of the processor validation parameters, which is essential for attaining a high data rate. It was discovered that a relatively well-defined optimum setting of the validation parameters may be determined, with the help of the real-time histogram display, by increasing the threshold values to the point where noise spikes appear occasionally with a maximum frequency of appearance of about 2%. The optimum threshold for the amplitude of the noise spikes may be determined by matching the noise floor of the velocity spectrum with either the Doppler-ambiguity noise or the discretization noise, whichever is greater. A set of commands may be entered via keyboard or execution of a command file to change the operating parameters of the processor and the traverse on-the-fly. The profiling FODLDV can be operated in an autonomous mode for days at a time by executing a command file in which the setup and operating parameters are sequentially specified.

The combination of the hardware and software has simplified and streamlined the application of laser anemometry to velocity measurement in general. Such improvements are essential for field deployment of LDVs. We have now eliminated most of the guesswork in setting up the LDV processor. With the help of the real-time histogram display of the Doppler frequency, not only the optimum threshold settings of the validation parameters but also the velocity range and/or resolution may be determined in situ with well-defined values. The post-processing software for noise-spike removal allows significant lowering of the threshold settings of the validation parameters such that weak bursts with marginal SNRs may be validated to assure a high data rate.

The modular profiling FODLDV consists of the following modules:

1. *The fiber-optic probe and link, which consist of a 1.6-cm-O.D., 18-cm-long aluminum cylinder and a 12-m-long water-tight armor cable.* The focusing and receiving optics, the collimating grin lenses coupled to three single-mode fibers, and the tip of the multimode fiber are housed in the aluminum cylinder. The fiber-optic probe is optically linked to the optronic module via four fibers

protected inside the armor cable. There are three single-mode fibers that transmit the Bragg-shifted laser light from the light source mounted in the optronic module and a multimode fiber that transmits the backscattered light from particles passing through the focal volume to the PMT.

2. *The optronic module.* This module consists of a miniature diode laser (made from a 830-nm, 100-mW single-mode laser diode on a heat sink with a TE cooler) driven by an ILX controller, a three-way beam splitter, three Bragg cells and drivers with crystal frequencies 80, 81, and 85 MHz, three fiber-optic couplers connected to the single-mode fibers, and a PMT (Hamamatsu R636) connected to the multimode fiber and power supplies.
3. *The digital FFT processor.* The FFT processor is based on the original chirp-Z Fourier transform processor developed by Agrawal and Belting (1988). Its two-channel DSP-based design has the flexibility of programmability that is capable of setting various operational parameters via a set of commands input via the keyboard or via the execution of a pre-edited command file. The FFT processor performs a 512-point FFT to determine the peak Doppler frequency. It has eight Doppler frequency or velocity ranges or resolutions designated by eight FFT windows 1 through 8 corresponding to TS 0 through 7. Table 1 details the conversion of the Doppler frequency and velocity for each window. The local oscillator may be changed to any value with a step of 488 Hz to facilitate asymmetric flows. The data sampling rates are programmable continuously from 10 to 200 Hz. For optimum operation of the FFT processor, the PMT should be overdriven to the extent that most strong bursts are saturated such that weak bursts would generate signals with good SNR, resulting in a high data rate.
4. *The DACS.* The DACS is a miniature 80386 25-MHz PC with a 100-Mbyte hard disk and a 1.44-Mbyte floppy for data I/O. The DACS has serial links to the FFT processor and to the traverse controller that allow both instruments to be operated via keyboard input or execution of a command file on the PC. Data acquisition programs were developed to conduct autonomously a sequence of experiments by operating the profiling FODLDV in a move-stop-and-sample mode. Data are automatically stored on the 100-Mbyte hard disk. While data are being recorded on disk, a histogram of the Doppler frequency can be displayed in real time on the screen to monitor the experiment in progress. Near-real-time display of the spectral distribution of the measured Doppler frequency is also available. These displays provide a preview of the velocity field to be measured and are useful tools for in-situ determination of the optimum setup for the velocity range and validation parameters of the FFT processor prior to recording.
5. *The mechanical traverse.* The traverse was designed to have a maximum range of 3 m with a resolution of 1 mm. The repeatability is 1 mm over the entire 3-m range. Provisions were made to mount the traverse and the FODLDV on a stationary platform and to operate in a move-stop-and-sample mode. The operation of the traverse is programmable by a set of commands that may be invoked via a serial link to the DACS. Autonomous operation of the traverse together with data acquisition and recording are accomplished by execution of a command file in which the operational parameters of both instruments are specified. The traverse may be modified to operate in a "yo-yoing" or a "wave-following" mode.

A set of software programs was developed for improving the application of laser anemometry in general, which is essential for field deployment of LDVs. For data acquisition and recording, the main program sets up the operational parameters for both the traverse and the FFT processor and invokes the data acquisition and recording procedure. A command file may be executed for autonomous operation of the profiling FODLDV until the 100-Mbyte hard disk is filled. In addition, there are subprograms for real-time display of the histogram of the Doppler frequency or near-real-time display of the spectral distribution. These two programs may be used to achieve optimum setup parameters such as the velocity range or resolution and the validation parameters of the FFT processor. There are several programs developed for post processing of the data: VALIDATA to extract the validated data points in the signal and the MMEDFILT to remove noise spikes in the LDV data. The MMEDFILT is a modified median filter with the incorporation of an acceleration criterion for identifying spikes to be removed. The MMEDFILT replaces a spike with the median value of its neighboring points but is edge preserving; it does not alter a spike-free time series. The implementation of the MMEDFILT has resulted in considerable improvement of the LDV setup by narrowing the range and lowering the value of the optimum thresholds of the validation parameters. It has been demonstrated that the optimum threshold corresponds to the occasional appearance of noise spikes in the time series (less than 1 to 2%). The lowering of the threshold ensures that weak Doppler bursts are validated, resulting in an increase in the data rate.

Laboratory tests were conducted to demonstrate the performance characteristics of the FODLDV. The combination of a short optical path, adequate laser power, a programmable and advanced FFT processor design together with real- and near-real-time data display, and the development of the modified median filter MMEDFILT for noise spike removal has led to a versatile, user-friendly, and field-worthy prototype FODLDV. For example, measurements in the oscillatory flow facility filled with tap water have shown a 92% data rate at 200 Hz. Such a high data rate in clean water without artificial seeding is necessary for turbulence measurements in the ocean. On the other hand, the short optical path minimizes blockage by particles in the flow, so that the FODLDV can also be used in turbid water. Our experimental results demonstrate several operational and performance features of the FODLDV that are superior to existing field-deployable and some laboratory LDV systems.

A series of field tests was also conducted in Luther Burbank Park, Mercer Island, located in Lake Washington in the Seattle area. The field worthiness of the profiling FODLDV in terms of logistics and operations has been successfully demonstrated. Further field tests are planned in order to extend laboratory demonstrations of the superior performance of the FODLDV to typical field conditions.

REFERENCES

Agrawal, Y. C. (1984) "A CCD Chirp-Z FFT Doppler Signal Processor for Laser Velocimetry," *Journal of Physics E (Scientific Instruments)*, Vol. 17, pp. 458-461.

Agrawal, Y. C., and Belting, C. J. (1988) "Laser Velocimetry for Benthic Sediment Transport," *Deep Sea Research*, Vol. 35, pp. 1047-1067.

Agrawal, Y. C., Aubrey, D. G., and Dias, F. (1988) "Field Observations of the Coastal Bottom Boundary Layer Under Surface Gravity Waves," presented at the Fourth International Conference on the Application of Laser Anemometry to Fluid Mechanics, Lisbon, Portugal, July 11-14.

Agrawal, Y. C., Hwang, P. H., and Pottsmith, H. C. (1991) "Velocity Structure of the Boundary Layer Under Waves in SUPERTANK," in preparation.

Brigham, E. O. (1974) *The Fast Fourier Transform*, Prentice-Hall, Inc., Englewood Cliffs, New Jersey, 252 pp.

Durst, F., Melling, A., and Whitelaw, J. H. (1976) *Principles and Practices of Laser Doppler Anemometry*, Academic Press, New York, 405 pp.

Gallagher, Jr., N. C., and Wise, G. L. (1981) "A Theoretical Analysis of Properties of Median Filters," *IEEE Trans. on Acoustics, Speech, and Signal Processing*, Vol. ASSP-29, No. 6. December, pp. 1136-1141.

George, W. K., and Lumley, J. L. (1973) "The Laser-Doppler Velocimeter and Its Application to the Measurement of Turbulence," *Journal of Fluid Mechanics*, Vol. 60, pp. 321-62.

Liu, H.-T. (1986) "Development of a Diode Laser Velocimeter with Directional Sensing Capabilities," Flow Technical Report No. 366, Flow Research, Inc., March.

Liu, H.-T. (1991) "Unsteady Aerodynamics of a Wortmann Wing at Low Reynolds Numbers," to appear in AIAA *Journal of Aircraft*.

Liu, H.-T., and Bondurant, P. D. (1988) "A Field-Worthy Diode Laser Doppler Velocimeter with Directional Sensing Capability: Prototype Development," Flow Research Report No. 450 (prepared for U.S. Department of Energy under Contract No. DE-AC03-85ER80244).

Liu, H.-T., and Lin, J.-T. (1987) "Measurements of Wave-Variance and Velocity Spectra in Breaking Waves," *Experiments in Fluids*, Vol. 5, pp. 201-212.

Liu, H.-T., Geller, E. W., and Cooper, M. (1985) "An Environmental Aerodynamic Test System for Low-Reynolds-Number Applications," *Proceedings of the Conference on Low Reynolds Number Airfoil Aerodynamics*, University of Notre Dame, Indiana, June, pp. 207-218.

Liu, H.-T., Kollé, J. J., and McPhee, M. G. (1985a) "Development of a Diode Laser Doppler Velocimeter for Measurements in the Oceanic Boundary Layer Under Ice" (abstract only), *EOS*, Vol. 66, No. 18, April.

Liu, H.-T., Kollé, J. J., and Bondurant, P. D. (1985b) "A High-Resolution Cluster of Oceanographic Instruments for Boundary Layer Measurements Under Ice," Flow Research Report No. 352, November.

Liu, H.-T., Kollé, J. J., and Bondurant, P. D. (1989) "Development of Field-Worthy Diode Laser Doppler Velocimeters," *Proceedings of Oceans '89*, September 18-21, Seattle, WA.

Pai, S. I. (1977) *Two Phase Flow* (K. Oswatitsch, Editor), Vieweg Tracts in Pure and Applied Physics, Vol. 3, Vieweg, & Sohn, Braunschweig, West Germany.

Schedvin, J. C., and Liu, H.-T. (1984) "The Development of a Diode Laser Doppler Velocimeter for Boundary Layer Measurements Under Ice: A Feasibility Investigation," Flow Technical Report No. 290.

Spectra Diode Labs (1988) "Laser Diode Operator's Manual and Technical Notes," Spectra Diode Labs, DCL 001 EB, November.

APPENDIX A
INSTRUCTIONS FOR USING THE FODLDV SOFTWARE

The FODLDV has three separate sets of software: the TMS320C25 assembly language software for the FFT processor, the 68HC000 software written in the "C" language for the FFT interface processor, and the IBM PC-compatible software, also written in "C," for the data acquisition and control computer. Each FFT processor has a program that resides in EPROM which executes an FFT on a time-sampled set of data and communicates over the G-96 bus connection with the 68HC000-based FFT interface processor. The operator does not interface directly with the DSP processor, but the commands sent to the 68HC000 processor configure and control the FFT conducted by the DSPs, so it is crucial that the operator understand how the DSPs operate.

The 68HC000 board is an MPL 4079 board made by Gespac that plugs into the G-96 bus. It controls the DSPs, reads the FFT data from them, stores the data, and sends the data back to the computer via a 19.2 Kbaud serial data link. This serial link uses 8 bits, no parity bit, and 1 stop bit. The 68HC000 program resides in EPROM.

The data acquisition and control computer is an IBM PC-compatible AMPRO Little Board 386. The FODLDV software to run on this computer is called pc.exe and is located in the C:\PC subdirectory. This software is executed by typing PC at the DOS prompt while in the C:\PC subdirectory. The program asks the user to enter the baud rate for communications with the 68HC000 board and then tells the user when communications have been established. Note that if the data acquisition and control computer has been rebooted after having previously executed pc.exe (without cycling the power), the baud rate has already been established with the 68HC000 processor and it is necessary to press the ESC key instead of selecting a new baud rate when starting the program. Once the baud rate has been selected and the initial sign-on message is complete the software checks the current directory to see if there are any command files. These are read and sorted into execution order by execution time. Command files with an execution time that has already passed are ignored. (However, if a file with the filename autoexec.cmd is present, it will be automatically executed immediately upon entering the program.) Up to 100 command files with the extension .cmd may be present. The command files will be executed at the appropriate time. The user may enter commands at the prompt at any time except when a command file is executing.

The following sample command file illustrates the file format:

```
execute at 11:22:33 on 06/24/91
he
cd 100 10
gte
```

The first line establishes when the file is to be executed. Subsequent lines are commands for either the 68HC000 card or for the GALIL motion control card. The syntax of the first line is crucial and cannot be varied.

The Ampro Little Board 386 (hereafter referred to as "the PC") uses one serial port (COM1) to communicate with the 68HC000 board and one (COM2) to communicate with the GALIL board, which controls the motion of the profiling traverse. GALIL commands are prefaced with a "G", while commands destined for the 68HC000 board are entered normally (note that there are no commands for the 68HC000 that begin with a "G"). Most commands are passed directly through the PC from the keyboard to the appropriate serial port. The responses from the GALIL card (serial port 2) are displayed in red, while those from the 68HC000 card (serial port 1) are displayed in green. Information from the PC's program is displayed in white. Certain commands to the 68HC000 card are intercepted by the PC, and appropriate action is taken. These commands are detailed below.

CD Used to collect data. When the **CD** command is given, the PC program sends the data sample rate and record length to the 68HC000 so it can begin to collect data, reads the system time, and saves it into an array to be stored until the data are uploaded from the 68HC000 card. This time stamp is then incorporated into the file where the data are saved when it is uploaded. The data collected after a **CD** command are stored locally until a **UD** command is executed.

UD Used to upload data. When the **UD** command is given, a file is opened for the storage of the data, handshaking with the 68HC000 is done to ensure that the correct data are sent to the PC, and a checksum is executed on the data sent to ensure that they are uncorrupted.

US Used to upload the current spectrum. When the **US** command is given, a file is opened to store the data, then a series of read data memory commands is sent to the 68HC000 card, which in turn sends them to the DSP currently in use. The data are read from the DSP and sent to the PC, which stores the data in the specified file.

PG Used to purge data. When the **PG** command is given, the PC ignores all previously collected data sets and starts over.

CU Used to collect and upload data. When the **CU** command is given, the PC opens a file for data storage and uploads all previous data sets, as well as the one initiated by this command. If histogram display is enabled, the histogram is shown while the data are collected. The histogram display is autoscaled after the collection is complete.

There are several commands unique to the PC. These are executed as alternate keystrokes (holding the "alt" key while pressing the other key). These commands are as follows:

Alt-A Enables display of a histogram of spectral peaks during a CU command. If timing data are being saved, then the validation bit will be checked. If a peak is valid, it is displayed in light blue; if a peak is invalid, it is displayed in red. If timing data are not saved, then all peaks are considered to be valid. When the collection is completed,

the data are redisplayed scaled to the value of the spectral bin with the most data points.

Alt-D Pushes to a DOS shell.

Alt-F Executes a command file that the user specifies.

Alt-G Directs keyboard output to serial port 2 (to the GALIL card).

Alt-H Displays the help menu.

Alt-N Disables displays during a CU command.

Alt-P Directs keyboard output to serial port 1 (to the 68HC000 board).

Alt-R Toggles whether raw data are saved in a binary format or converted to ASCII.

Alt-S Displays spectrum uploads continuously.

Alt-V Displays a real-time velocity chart during a CU command (NOT IMPLEMENTED).

Alt-X Ends the program.

Pressing the space bar causes one spectrum to be loaded and displayed on the screen.

Escape ends the program.

A listing of complete command descriptions is provided on the following pages.

Command Set

command syntax	description	68HC000 response
HE	help	Displays a list of the commands together with short descriptions.
SP XXXX	set program address	Sets address for read or write in DSP program memory. Also returns value for DSP program memory address to the PC in the format XXXX<CR>.
RP	read program memory and increment address	Returns data to the PC in the format XXXX<CR>.
RP XXXX	read program memory and set address	Sends RP command to DSP. When transaction with DSP complete, sends the data back to the PC in format XXXX<CR>.
WP XXXX	write program memory and increment address	Sends WP command to DSP. When transaction with DSP complete, sends <CR> back to PC. Note that address must be set first.
SD XXXX	set data memory address	See SP above.
RD	read data memory and increment	See RP above.
RD XXXX	read data memory	See RP above.
WD XXXX	write data memory and increment	See WP above.
SI XXXX	set I/O address	See SP above.
RI	read I/O and increment	See RP above.
RI XXXX	read I/O	See RP above.
WI XXXX	write I/O and increment	See WP above.
SR XXXX	set register	See SP above.
RR	read register and increment	See RP above.
RR XXXX	read register	See RP above.
WR XXXX	write register and increment	See WP above.
BG XXXX	begin program execution at address	Sends BeGin command to DSP. NOT YET IMPLEMENTED
SB XX	set board	Allows the user to designate which DSP board is addressed. The address of the DSP board is entered (replaced by UB now).
DB D	disable board	Disables board D so it is not used.
EB D	enable board	Enables board D for use.
UB D	use board	Same as SB except the board number is used.
DL	download program	68HC000 will expect that the next thing it sees will be the beginning of the ti tag format file.

command syntax	description	68HC000 response
CD DDD DD	collect data	68HC000 will be begin collecting data from the DSPs and storing it in the 68HC000. DDD is the frequency sample rate in hertz (10 to 200Hz); DD is the number of seconds to sample (maximum of 255). If CD<CR> is sent, then the previously used rate will be used (or the default will be used if no previous rate was set).
CU DDD DD, name	collect data and upload it to the PC	68HC000 will be begin collecting data from the DSPs and sending them back to PC. DDD is the frequency sample rate in hertz (10 to 200Hz), DD is the number of seconds to sample (maximum of 255). "name" is the name of the file in which the data will be saved. If CU<CR> is sent, then the previously used rate will be used (or the default will be used if no previous rate was set). If enabled with Alt-A, a histogram display will be shown while the data are uploaded.
SS	single sample	A single sample is read from the DSPs and displayed on the terminal.
UD name	upload data	Sends all saved data sets to the PC, which places the data into a file called "name."
PG	purge data	Resets all data pointers to their original values, without uploading the data.
US name	upload spectrum	Sends the current spectrum to the PC, which places the spectrum data into a file called "name."
NT	time data disable	Disables the saving of time data from the DSP.
TD	time data enable	Enables the saving of time data from the DSP. Must be enabled for the burst validation criteria to be applied.
ST	status	Displays a status report of which DSPs are currently being used, RAM storage space used and available, and whether or not time data are being stored.
SL DDD	set spectral level	Allows the user to set the spectral threshold (minimum value for a burst to be considered valid).

command syntax	description	68HC000 response
AO ON or AO OFF	enable analog output	Enable or disable output of analog display of FFT spectrum.
ST DD	set threshold	Allows the user to modify the burst amplitude threshold using a decimal number. 0 = 0 V, 99 = +2.5 V
SV DD	set validation level	Allows the user to set the spectral signal-to-noise-ratio threshold. A value of 10 means that a spectral peak must be ten times higher than the average value of the spectrum to validated.
MF D	maximum frequency D = 0 to 3	Sets the burst digitization rate on the FFT processor. It also sets the programmable filters and oscillators on the demodulator card. Combines commands TS, O1, O2, F1, and F2. The following table shows the breakdown: MF O1 O2 0 1.250 MHz 4.250 MHz 1 1.125 MHz 4.125 MHz 2 1.0625 MHz 4.0625 MHz 3 1.03125 MHz 4.03125 MHz MF F1 & F2 TS 0 33 (500 kHz) 0 (1 MHz) 1 22 (250 kHz) 1 (500 kHz) 2 11 (125 kHz) 2 (250 kHz) 3 00 (62.5 kHz) 3 (125 kHz)
TS D	time sample D = 0 to 7	Sets the burst digitization rate on the FFT processor card. 0 = 1 MHz 1 = 500 kHz 2 = 250 kHz 3 = 125 kHz 4 = 62.5 kHz 5 = 31.25 kHz 6 = 15.625 kHz 7 = 7.8125 kHz

command syntax	description	68HC000 response
O1 DDDDDDD	set oscillator 1 Valid values can range from 0 to 32000000. The actual oscillator frequency will be an integer multiple of 488.28 Hz.	Allows the user to set the programmable oscillator 1 on the demodulator card to a desired frequency DDDDDDD (replaces N1). For a given TS value the appropriate O1 for a symmetrical flow is: TS O1 (DDDDDD) 0 1250000 1 1125000 2 1062500 3 1031250 4 1015625 5 1007813 6 1003906 7 1001953
O2 DDDDDDD	set oscillator 2	Same as O1 but for oscillator 2. To determine the appropriate 02 value for a given TS value, add 3 MHz to the values given for O1.
N1 XX	set NCO 1	Allows the user to set oscillator 1 using the register on the chip (replaced by O1).
N2 XX	set NCO 2	Allows the user to set oscillator 2 using the register on the chip (replaced by O2).
F1 XX	set filter 1 and filter 2 XX = 0 to 3	Allows the user to set filter 1 and 2. Bits 0 and 1 set Filter 1 and bits 4 and 5 set Filter 2. For both filters the bits correspond to the following table: 11 (3) = 500 kHz 10 (2) = 250 kHz 01 (1) = 125 kHz 00 (0) = 62.5 kHz
F2 XX	set filter 1 and filter2	Same as F1.

NOTE: in all cases 68HC000 checks command syntax first and, if there is an error, responds with ?; otherwise, 68HC000 responds with ! followed by the above response. XXXX refers to a four-digit (16 bit) hexadecimal number; DDD refers to a three-digit decimal number.

68HC000-to-FFT-Processor Commands

The FFT processor occupies three registers across the G-96 bus: data registers 1 and 2 (DR1 and DR2) and the command register (CMD)

command syntax to DSP registers	description	DSP response
DR1 XX (high byte of address) DR2 XX (low byte of address) CMD 11	set program memory address for either reading or writing	DSP interprets CMD. Reads address in DR1 and DR2. Stores address. Fetches data. Puts data in DR1 and DR2. Writes EE (inverse 11) to CMD.
DR1 nothing changed DR2 nothing changed CMD 21	read program memory and increment address	DSP interprets CMD. Fetches data. Puts data in DR1 and DR2. Increments stored address. Writes DE (inverse 21) to CMD.
DR1 XX (high byte of data) DR2 XX (low byte of data) CMD 31	write program memory and increment address	DSP interprets CMD. Reads data in DR1 and DR2. Stores address. Writes CE (inverse of command) to CMD.
DR1 XX (high byte of address) DR2 XX (low byte of address) CMD 12	set data memory address for either reading or writing	DSP interprets CMD. Reads address in DR1 and DR2. Stores address. Fetches data. Puts data in DR1 and DR2. Writes ED (inverse 12) to CMD.
DR1 nothing changed DR2 nothing changed CMD 22	read data memory and increment address	DSP interprets CMD. Fetches data. Puts data in DR1 and DR2. Increments stored address. Writes DD (inverse 22) to CMD.
DR1 XX (high byte of data) DR2 XX (low byte of data) CMD 32	write data memory and increment address	DSP interprets CMD. Reads data in DR1 and DR2. Stores address. Writes CD (inverse 32) to CMD.
DR1 XX (high byte of address) DR2 XX (low byte of address) CMD 10	set I/O port address for either reading or writing	DSP interprets CMD. Reads address in DR1 and DR2. Stores address. Fetches data. Puts data in DR1 and DR2. Writes EF (inverse 10) to CMD.

command syntax to DSP registers	description	DSP response
DR1 nothing changed DR2 nothing changed CMD 20	read I/O port and increment port address	DSP interprets CMD. Fetches data. Puts data in DR1 and DR2. Increments stored address. Writes DF (inverse 20) to CMD.
DR1 XX (high byte of data) DR2 XX (low byte of data) CMD 30	write I/O port and increment port address	DSP interprets CMD. Reads data in DR1 and DR2. Stores address. Writes CF (inverse 30) to CMD.
DR1 XX (high byte of address) DR2 XX (low byte of address) CMD 40	start program execution at address. NOT IMPLEMENTED	DSP interprets CMD. Reads address in DR1 and DR2. Writes BF (inverse of command) to CMD. Starts program from there.
DR1 nothing changed DR2 nothing changed CMD 50	collect data	DSP interprets CMD. Dumps previous FFT in DR1 and DR2. Writes AF (inverse of command) to CMD. DSP reads FIFO, enables threshold detector, begins FFT crunching.
DR1 XX (high byte of data) DR2 XX (low byte of data) CMD 60	set threshold	DSP sets threshold.
DR1 0 for OFF, non-0 for ON DR2 0 for OFF, non-0 for ON CMD 70	enable analog output	DSP enables analog output. (The analog output cord must be connected.)
DR1 0 DR2 0 to 7 CMD 80	set time sample	DSP sets time sample.
DR1 XX (high byte of data) DR2 XX (low byte of data) CMD 90	set validation level	DSP sets validation level.

APPENDIX B
TRAVERSE CONTROLLER COMMAND SET

The DMC-100 provides an extensive instruction set for programming a variety of motion profiles. An instruction consists of two letters, followed by an applicable parameter number. All instructions are uppercase and sent one character at a time in ASCII. A semicolon or carriage return terminates the instruction. Example: PR 4000; PR is the 2 character instruction code for position relative. 4000 is the parameter which represents the required position value. The ; terminates the instruction. The instructions are grouped according to function and described below. The commands noted with the # can be applied while the motor is moving.

Control Parameters

GN n - Gain of digital filter #. Range: 0-255, except for 1

ZR n - Zero of digital filter #. Range: 0-255

PL n - Pole of digital filter #. Range: 0-255

KI n - Integrator of digital filter #. Range: 0-127

DB n - Deadband of ±n #. Range: 0-127

OF n - Offset of ±n #. Range: 0-127

TM n - Controller sample time in microseconds. Range: 500-65000

TL n - Torque limit. Limits the output voltage to the range between -10·n/128 and 10·n/128. If motor cannot run at specified speed due to TL limit, the commanded speed slows down in order to limit the position error to 1024 #. Range: 0-127

# denotes that command can be applied while motor is moving.

Control Modes

SV - Servo Mode. System controls the position and corrects for errors continuously.

SH - Servo Here. Enables transition from Motor Off (MO) to servo mode. Current motor position is defined as desired position.

MO - Motor-Off Mode. The position is monitored continuously but the motor command is turned off. This mode is useful when the motor shaft has to be turned manually. Use SV to return to the original command position or SH to servo at the current position.

VM n - Velocity Mode. Specify parameter to define speed magnitude and direction. # Range: 4 to ±250000 counts/sec. Resolution is 4 counts/sec. Note: The actual speed is 1000/1024 of the command speed.

DH n - Defines the current and commanded position specified by n. Range: $\pm 8 \times 10^6$

SN n - Stop from Run. Stops motion a distance n counts after a low input on the start/stop line. Accuracy is SP/2000. n must be greater than $SP/2000 + SP^2/2*AC$. #

FE - Find Edge. This command is used to reference the system to an external switch. Following the FE and BG command, the motor

slews at the specified speed until a transition occurs on the direction switch (Pin 12 of J1). The direction of motion is defined by the initial level of the direction switch.

IM - Incremental Mode. Allows arbitrary position trajectory to be specified. Disables controller profiler. Use IM to specify mode. Use 80 hex to terminate mode. While in the incremental mode, controller can receive only position increment values and no other communication can be performed.

Profiling Parameters

PR n - Specifies target distance of n counts relative to current command position. Units are quadrature counts. Range: $\pm 8 \times 10^6$

PA n - Specifies target position to absolute position, n. This position is referenced from the absolute zero. Range: $\pm 8 \times 10^6$

SP n - Specifies speed rate in counts/sec for velocity and position mode. Resolution is 4 counts/sec. Range: 0-250000
Note: The actual speed is 1000/1024 of the commanded speed.

AC n - Specifies acceleration and deceleration rate in units of counts/sec^2. Resolution is 4096 counts/sec^2. (# when in VM mode). Range: $0\text{-}1.3 \times 10^8$

DF - Specifies direction as FWD in VM mode.

DR - Specifies direction as REV in VM mode.

DS n - If n=1, direction of motion is specified by direction input (Pin 12 of J1). The Forward direction is a low input, Reverse is high. Range: 0 or 1

IP n - Increment Position. Command new position while the motor is in motion. This command does not work in the velocity mode (VM). The polarity of n must be in the same direction of motion. # Range: $\pm 8 \times 10^6$

Start/Stop

BG - Begins motion for PR, PA, VM, FE modes.

ST - Stops motion. Causes motor to decelerate to a stop. #

AB - Stops motion instantaneously without deceleration. #

RP n - Repeats PR motion n times in the same direction. If n=0, the motion sequence is repeated indefinitely. Use n=1 to terminate mode. Range: 0-255

RR n - Repeats PR motion n times with direction alternated. If n=0, the motion sequence is repeated indefinitely. Use n=1 to terminate mode. Range: 0-255

WT n - Wait n msec between RP or RR motion repetitions. # Range: 0-32000

SS n - Start motion on switch if n=1 and when stop/start* input (Pin 10 of J1) goes low following BG command. SS0 disables function. Range: 0 or 1

ES n - End motion in switch of n=1 and when stop/start* input (Pin 10 of J1) goes high. Range: 0 or 1

OE n - Off-on-Error. Turns the motor command off when n=1 and the position error exceeds that specified by the ER error limit. This mode is motor-off, MO. Use SV or SH to turn the motor back on. n=0 turns off the off-on-error feature. # Range: 0 or 1

Numbering System

DC - Input numbers in decimal, output in HEX. #

HX - Input in HEX, output in HEX. NOTE: Negative numbers are input as signed negative numbers. #

Interrogate

TP - Tell Position. Reports the absolute position as a 6 digit hexadecimal number. 2's complement. #

TE - Tell Error. Reports the position error as a 4 digit hexadecimal number. 2's complement. #

TV - Tell Velocity. Reports actual motor velocity as 6 digit hexadecimal number. 2's complement. This output is rounded to the nearest 2048 counts/sec. #

TI - Tell inputs and status. In response, the system reports a 2 digit hexadecimal number. The 8 decoded bits represent the following status. #

Bit 7	Executing Sequence*
6	Executing Move*
5	FWD limit switch*
4	REV limit switch*
3	Remote/local*
2	Stop/start* input
1	Direction input REV/FWD*
0	Excessive position error

TT - Tell Torque. Reports the motor command as a 2 digit, 2's complement number. #

Example:

TT Response	Motor Command
80	-10V
FF	-0.08V
00	0
7F	10V

TC - Tell Code. Allows the user to determine why the motor stops. The controller responds with the stop code as follows: #

Code	Meaning
00	Motor is running, no stop command received
01	Stopped at commanded position
02	Decelerating or stopped by FWD limit switch
03	Decelerating or stopped by REV limit switch
04	Decelerating or stopped by Stop Command (ST)
05	Decelerating or stopped by End-on-Switch (ES1)
06	Stopped by Abort Input
07	Stopped by Abort Command (AB)

08	Decelerating or stopped by Off-on-Error (OE1)
09	Stopped after finding edge (FE)
10	Stopped n counts from input (SN n)
11	Stopped after input, but n too small (SN n)

RD n - Reports "H" to the command port when motion command is complete and if n=1. Range: 0 or 1

TS - Reports the latched position captured with LT 1 command. #

PD n - Position Dump. If n=1, position reporting mode activated. Change in position from previous sample is reported every sample. The range of numbers is between -127 and 127. The numbers are reported as a single byte. It is the responsibility of the user to read the reported position every sample period. In the reporting mode, the controller may receive commands, but will not send responses to them. For example, ST stops the motion while TP results in no response. Position reporting is stopped with PD 0.

Other

SM n - Sign Magnitude. Sets the mode of the motor command. When n=0, the PWM output is 0% duty cycle for full negative voltage, 50% for 0 voltage and 99.6% for full positive voltage. When n=1, the PWM signal is 0% for 0 voltage, 99.6% for full voltage and the sign of the motor command is available at the sign output. Range: 0 or 1

RS - Resets the controller to default values. All position counters are initialized to zero.

ER n - Error Limit. Specifies the position error limit as ±n counts. Whenever this limit is exceeded, the error output will indicate that. # Range: 0-1023

LT n - Latch Position. n=1 arms position latch. Captures motor position if the start/stop input is held low for a minimum of .5 msec. Once the position is latched, the function is disarmed. Read latched position with TS command. # Range: 0 or 1

Interrogate

It is possible to interrogate the system with the commands:

```
TQ?  Report torque command level  #
GN?  Report gain  #
ZR?  Report zero  #
PL?  Report pole  #
DB?  Report deadband  #
OF?  Report offset command level  #
```

Default Parameters

Upon reset, the system starts in a position control servo mode.

SV

If the MOF is jumpered, the default mode is motor off.

MO

The digital filter default values are GN=8, ZR=232, PL=0, and KI=0.

The motor command mode is bipolar

SM(n), n=0

and the default values of the speed and acceleration are

SP = 32768

AC = 65536

APPENDIX C

VALIDATA AND MMEDFILT SOURCE CODE

LISTING OF VALIDATA.M

```
% Program "validata.m"
%*****************************************************************************************************
% This program extracts the validated data points from the raw FODLDV file
% The input file "turaw" is a two-column file. The first column is
% the number of time bins from the start of each sampling window plus a validation code 128
% The second column is the frquency bin number in which the Doppler frequency falls
% n(1) is the total number of raw data points
% n(2) is the target sampling rate of the time series
% n(3) is the zero velocity bin
% n(4) is the frequency bin width
%*****************************************************************************************************
%@@@@@@@@@@@@@@@@@@@@@@@@@@@@@@@@@@@@@@@@@@@@@@@
%                    Programmed by (Peter) H.-T. Liu
%                    Quest Integrated, Inc.
%                    21414 68th Avenue South
%                    Kent, Washington 98032
%                    Telephone: 206-872-9500
%                    Last revision: November 5, 1991
%@@@@@@@@@@@@@@@@@@@@@@@@@@@@@@@@@@@@@@@@@@@@@@@
i1=0;
i2=0;
for i=1:n(1),
    if (turaw(i,1) >= 128),
        i1=i1+1;
        tu(i1,1)=(turaw(i,1)-128)*.0005+(i-1)/n(2);
        tu(i1,2)=(turaw(i,2)-n(3))*n(4);
    end
end
```

LIST OF FUNCTION MMEDFILT

```
function out = medfilt(x, len, p)
%*************************************************************************************
% Processes LDV data for spike removal with a running
%    modified median filter
% A spike is removed when the product of its amplitude and the sampling rate
%    exceeds the maximum acceleration physically sustainable in the flow
% Usage: mmedfilt(x, len, p)
%              x = vector to be filtered
%            len = median filter length (normally an odd number)
%              p = amplitude of spikes to be removed
%*************************************************************************************
%@@@@@@@@@@@@@@@@@@@@@@@@@@@@@@@@@@@@@@@@@@@@@@@@@@@@@@@
%          Programmed by Phil Bondurant and revised by (Peter) H.-T. Liu
%                Quest Integrated, Inc. 21414 68th Avenue South
%                          Kent, Washington 98032
%                          Telephone: 206-872-9500
%                        Last revision November 5, 1991
%@@@@@@@@@@@@@@@@@@@@@@@@@@@@@@@@@@@@@@@@@@@@@@@@@@@@@@@
[m,n] = size(x);
if ((n > 1) & (m > 1))
  disp('Error: input data must be a row or column vector');
else
if (n == 1)
x=x';
out=x;
end
  endlength = fix(len/2);
  temp = [zeros(1, endlength)+x(1) x zeros(1, endlength)+x(length(x))];
    i = find (abs(diff(x)) > p);
    for j = 1 : length(i),
      out(i(j)) = median(temp(i(j):i(j)+len-1));
    end
    out=out';
end
```